University of California
Los Angeles

Biomechanical Simulation of the Human Hand and Forearm

A thesis submitted in partial satisfaction
of the requirements for the degree
Master of Science in Computer Science

by

Wilson Yan

2012

The thesis of Wilson Yan is approved.

Stefano Soatto

Michael G. Dyer

Demetri Terzopoulos, Committee Chair

University of California, Los Angeles

2012

Table of Contents

1 Introduction **1**

1.1 Thesis Contributions 2

1.2 Thesis Overview 3

2 Previous Work **4**

2.1 Inverse Kinematics 4

2.2 Biomechanical Simulations 6

2.2.1 Muscle Simulations 7

3 Musculoskeletal Design **9**

3.1 Rigid Bodies and Joints 9

3.2 Muscle Model 10

3.2.1 B–Spline Representation 11

3.2.2 B–Spline Control Points 12

3.3 Forward Dynamics Simulation 13

3.3.1 Hill–Based Muscle Model 13

3.3.2 Manual Activations 14

4 Implementation **15**

4.1 Open Dynamics Engine 15

4.2 OpenSceneGraph 16

4.2.1 Rigid Bodies 16

4.2.2 Joints 16

4.2.3 Muscle Control Points 17

4.2.4 Node Callbacks 17

5 Simulation Results and Analysis 19

5.1 Thumb 20

5.2 Index Finger 21

5.3 Middle Finger 22

5.4 Ring Finger 22

5.5 Little Finger 23

5.6 Wrist 24

5.7 Analysis 26

6 Conclusion 30

6.1 Future Work 31

A Anatomy 33

A.1 Bones 33

A.2 Bones and Muscles from the Ultimate Human Model 34

A.3 Muscles 38

A.3.1 List of Muscles 38

A.3.2 Hand Muscles 39

A.3.3 Wrist Muscles 44

B Bone Hierarchy 45

C Muscle Control Points 46

Bibliography 52

List of Figures

5.1 Rest pose 19

5.2 Flexion/Extension of the thumb 20

5.3 Flexion/Extension of the index finger 21

5.4 Flexion/Extension of the middle finger 23

5.5 Flexion/Extension of the ring finger 24

5.6 Flexion/Extension of the little finger 25

5.7 Wrist muscle attachments 26

5.8 Flexion/Extension/Abduction/Adduction of the wrist 27

A.1 Skeletal structure of the human hand and forearm 33

A.2 Right lateral view of the hand 34

A.3 Top view of the hand 35

A.4 Left lateral view of the hand 36

A.5 Bottom view of the hand 37

A.6 Hand upper muscles 39

A.7 Finger upper muscles 40

A.8 Hand lower muscles 41

A.9 Finger lower muscles 42

A.10 Thumb muscles 43

A.11 Wrist muscles 44

List of Tables

5.1 Thumb muscle lengths at different poses 20

5.2 Index finger muscle lengths at different poses 22

5.3 Middle finger muscle lengths at different poses 22

5.4 Ring finger muscle lengths at different poses 23

5.5 Little finger muscle lengths at different poses 24

5.6 Wrist muscle lengths at different poses 25

A.1 Muscle groups and names 38

B.1 Bone hierarchy 45

C.1 Thumb muscle control points 46

C.2 Index finger muscle control points 47

C.3 Middle finger muscle control points 48

C.4 Ring finger muscle control points 49

C.5 Little finger muscle control points 50

C.6 Wrist muscle control points 51

Acknowledgments

I am grateful to Professor Demetri Terzopoulos for being my thesis supervisor. The discussions I had with him taught me a great deal about biomechanical systems and provided valuable guidance on the ideas behind this thesis. Thanks to his careful and detailed reading of thesis drafts, I have learned a great deal about good writing structure and style.

I am thankful to Professors Michael G. Dyer and Stefano Soatto for comprising the remainder of my thesis committee and reviewing my thesis.

Craig Jessen and Steve Arbuckle provided helpful assistance with administrative issues and paperwork in the Computer Science Department.

I am grateful to Sung-Hee Lee for his informative insights into my research and for providing the *Ultimate Human* model of the musculoskeletal system. Additionally, the open source 3D viewing program *Blender* allowed me to use the 3D geometries of the *Ultimate Human* model and generate muscle control points, and the open source toolkits *OpenSceneGraph* and *Open Dynamics Engine* enabled me to develop the biomechanical hand simulation environment.

I am greatly indebted to Jonathan Fredeluces Garcia for being an amazing partner in our original course project on modeling the hand. Without his contributions to that project and the accompanying report, this thesis would not have been possible.

I am deeply grateful to Mary Conradt for being an inspirational co-worker, a wise friend, and a genuinely kind person. Her encouragement and guidance has allowed me to mature and attain goals that I never thought I would be able to achieve. I am grateful to Susy Chang and Melva Guzman for their unwavering friendship throughout the years and for their confidence in me, as well as to Mary Huang, Charles Chen, Noah Kagan, and Cindy Zhou for the kindness, friendship and companionship that they have provided me during my graduate years.

Finally, I am thankful for my family—my parents Situ Huijuan Yan and King Man Yan, my brother Jason Victor Yan, and my sister Lisa Yan—whose love and support throughout my life has helped me to follow the path I set before me.

Abstract of the Thesis

Biomechanical Simulation of the Human Hand and Forearm

by

Wilson Yan

Master of Science in Computer Science

University of California, Los Angeles, 2012

Professor Demetri Terzopoulos, Chair

In computer graphics, biomechanics has been pursued by researchers in recent years as a means of addressing the difficult challenge of physically realistic human character animation. In this context, this thesis presents a system that simulates a biomechanical model of the human hand and forearm in order to animate realistic hand gestures through forward dynamics. In our implementation, bones are simulated as passive rigid bodies and muscles as massless uniform cubic B-splines. Our biomechanical model employs accurate bone geometries and emulates the complex muscle routings of the human hand. Each muscle is a contractile actuator that applies forces to associated bones in order to articulate the jointed skeletal structure of the hand. In this manner, our simulator produces realistic hand animations, which further support the use of biomechanics in character animation and can also provide insights into the dynamics of the human hand.

CHAPTER 1

Introduction

According to Hodgkinson (2009), one of the ultimate goals of animation is to convey an "illusion of life" or realism to the viewers. Unlike 2D animation, 3D computer animation has the advantage of realism through 3D rendering. The realism that 3D rendering offers is constantly growing as research and development in graphics hardware and software advances. However, realism in computer animation does not depend solely on the quality of the rendering, as character animation also plays a crucial role in conveying realism.

In traditional character animation, expert animators have the task of generating character movement through the process of keyframing. Forward and inverse kinematics are two techniques that are commonly used in this process. In interpolating between keyframes, forward and inverse kinematics are employed to adjust the object's joints and orientations to the values specified by the animators. Ultimately, the expert animators are left with the task of creating perceptually realistic animations through their experience and expertise in the field. Keyframing realistic animations can be difficult and time-consuming. As a direct result, alternative methods for generating realistic animations have been and continue to be researched.

An important approach to generating the desired perceptual realism is the incorporation of physics into computer animation. Biomechanical models for animation strive to synthesize lifelike motion by simulating the relevant physical properties of the real world. Unlike the models used in forward and inverse kinematics, the bones in a biomechanical model are passive rigid bodies that move when forces are applied to them. The forces produced by the muscles actuate the bones such that they rotate around joints.

This thesis describes a technique and implementation process for creating a biomechanical simulation of the human hand and forearm, which is capable of producing realistic hand animations. Unlike for inverse kinematics, the joint angles and orientations of bones need not be specified by the animator. Instead, our simulator requires animators to specify the muscle activations, which will induce the muscles to produce contractile forces. These forces are then applied onto the joint skeletons, actuating the bones in which the muscles originate and insert such that they rotate to produce the desired skeletal joint angles.

Our forward dynamic simulation utilizes a simplified human hand and forearm model. This model includes 30 human bones, but for simplicity this is reduced to 16 different rigid bodies by grouping some of the bones together as individual rigid bodies. The human hand and forearm contains over 60 muscles, but we simulate only 25 of them. Despite our simplifications, the fingers and thumbs of our biomechanical model are able to simulate flexion and extension and the wrist can simulate flexion, extension, abduction, and adduction. Other movements of the fingers and thumbs, such as abduction/adduction, and pronation/supination for the wrist, are not simulated by our system.

1.1 Thesis Contributions

The contributions of this thesis are as follows:

- A biomechanical hand model that closely resembles a human left hand, particularly with realistic geometric bone models and anatomically accurate muscle routings that follow the paths of real muscles.

- A forward dynamic simulator that is capable of producing a variety of hand motions.

Although our simulator uses simplified models, it nonetheless provides insights into techniques for developing realistic character animations through biomechanical modeling as well as provide a better understanding of the biomechanics of the human body. Furthermore, the different hand motions resulting from the simulation show the promise of the forward dynamics approach relative to forward and inverse kinematic systems.

1.2 Thesis Overview

The remainder of this thesis is organized as follows: Chapter 2 reviews relevant prior work on the methods of forward and inverse kinematics, biomechanical models, and different types of muscle modeling. Chapter 3 describes the biomechanical model design of the bones, muscles, and forward dynamics. Chapter 4 describes the simulation design and implementations used in our system. Chapter 5 gives the results and analysis of our simulator's ability to produce realistic hand motions. Chapter 6 discusses approaches for improving the simulation.

CHAPTER 2

Previous Work

There is an enormous amount of literature regarding computer animation. In this chapter, we will focus particularly on the topics relevant to character animation and modeling. First, we will review inverse kinematics, improvements on this technique, and customizations of this technique for specific applications. Next, we will review work on biomechanical simulations that are relevant to musculoskeletal designs. Finally, we will look at relevant work on modeling and simulating muscles.

2.1 Inverse Kinematics

Inverse kinematics has long been the main technique for generating motion/movement of articulated objects, and significant research has been done on improving and customizing this technique to fit specific needs.

There have been numerous studies in improving inverse kinematic solvers by modifying the algorithm to improve its efficiency. Ho et al. (2005) suggested the approach of using linear programming to solve inverse kinematics problems for multi-body systems. This variant of the algorithm allowed the computations to be efficient as they grew linearly with the number of degrees of freedom and constraints. Conversely, a non-linear approach was suggested as an efficient solver for highly articulated models in (Zhao and Badler, 1994). These improvements on inverse kinematics focused primarily on the programming optimizations of the algorithm.

Other approaches focused on speed and versatility, particularly by making use of case based scenarios. Fêdor (2003) implemented an inverse kinematics solver for skeletal manipulation that switches between three inverse kinematic algorithms, depending on which one is fastest for the current situation: algebraic, iterative optimization using Newton-Raphson, and Cyclic Coordinate Descent. Lee and Shin (1999) describe an inverse kinematics solver that switches between two algorithms based on the articulated object's tree hierarchy: one algorithm for general-tree structured objects and the other for objects with human-like limb linkages. Both of these approaches employ different algorithms within the inverse kinematic solver based on the constraints and situation of the given problem. Similarly, by using multiple processors to target different independent inverse kinematic problems at once, a parallel inverse kinematics system was able to solve the inverse kinematic problem in a fast and efficient manner (Lai and Chao, 1989).

Many authors have also customized the inverse kinematics algorithm to fit their specific application needs. Sumner et al. (2005) describe a mesh-based inverse kinematics algorithm that can produce meaningful deformations over a large mesh. Der et al. (2006) present a new inverse kinematic algorithm for reduced-deformable models, allowing models to properly deform without the need for animators to worry about the deformations. Some inverse kinematic systems allow for stylizing and customizing, based on the specific training data (Meredith and Maddock, 2005; Grochow et al., 2004). Peinado et al. (2007) describe an inverse kinematic system that works directly with collision control, allowing the models to avoid collision with other objects.

Since it is a well-known and commonly used technique, there is no doubt that inverse kinematics will attract further research. However, despite its popularity, animators must still set the object constraints and go through the process of keyframing in order to generate desired animations. Thus, this thesis will investigate the alternative method of forward dynamics and simulation for computing character movement.

2.2 Biomechanical Simulations

There has been a significant amount of research on biomechanical simulations in the graphics community. A large portion of these efforts include physics-based and musculoskeletal systems. One of the greatest benefits of biomechanical studies is the realism that they add to the simulation.

Several papers present biomechanical models of animals. McKenna and Zeltzer (1990) introduce a simple biomechanical model of a six-legged figure, a simulated insect. Wu and Popović (2003) describe the modeling of a bird with an articulate skeleton and the dynamics behind the bird's wing beat motion. Simmons et al. (2002) describe the modeling and animation of a canonical horse. Tu and Terzopoulos (1994) present a biomechanical model of fishes.

The majority of biomechanical animation techniques focus on human models, or specific parts of the human body. Some have focused just on the musculoskeletal anatomy and not the associated dynamics (Scheepers et al., 1997; Wilhelms and Gelder, 1997). Others have focused only on the physics-based animation aspect of the biomechanics (Faloutsos et al., 2001; Pollard and Zordan, 2005). A few papers discuss modeling bipedal locomotion (Easterling et al., 2011; Yin et al., 2007). Extensive studies have been made on using musculoskeletal models for facial animation, particularly in simulating facial expressions (Sifakis et al., 2005; Lee et al., 1995). Zordan et al. (2004) developed a human torso model that uses spring-based muscles to simulate human respiration. Lee and Terzopoulos (2006) simulated the human neck and implemented a neuromuscular controller that learns to balance the mass of the head atop the cervical column and produces realistic head movements. A highly detailed modeling and biomechanical simulation of the musculoskeletal anatomy of the human upper body was achieved by Lee et al. (2009).

More closely related to the topic of this thesis, several papers consider the modeling of the human hand along with simulating different hand motions and gestures (ElKoura and Singh, 2003; Albrecht et al., 2003; Sueda et al., 2008). Sueda et al. (2008) simulated a musculotendon simulation for the human hand that also produces detailed skin deformations.

2.2.1 Muscle Simulations

Within the designs of musculoskeletal systems, muscles have been simulated in many different ways. Several papers in the literature have employed thin physical strands for simulating muscles as force actuators (Lee and Terzopoulos, 2006; Lee et al., 2009; Sueda et al., 2008). Zordan et al. (2004) simulated muscles as strands with spring-based elements. To add muscle volume, some simulations model muscles with ellipsoids, which allows for deformation of muscles when contracting and relaxing (Scheepers et al., 1997; Pratscher et al., 2005). Audenaert and Audenaert (2008) emphasize the importance of modeling muscles with routings that can wrap around obstacles, rather than with straight lines. Wilhelms and Gelder (1997) modeled muscles with deformed-cylinders and Zhou and Lu (2005) used NURBS to model muscles with volume. Other approaches include the use of finite volume methods to simulate skeletal muscles by Teran et al. (2003).

In this thesis, muscles are modeled primarily for driving the forward dynamics of the simulation. At the same time, the muscles will follow the complex routing of real hand muscles, allowing the simulation to closely mimic that of a real human hand. For simplicity, the muscles are modeled as B-splines, rather than muscles with volumetric properties.

CHAPTER 3

Musculoskeletal Design

Our forward dynamic simulation of the human hand consists of two basic components: bones and muscles. The bones are modeled as passive rigid bodies (Section 3.1) and the muscles are modeled by massless uniform cubic B-splines (Section 3.2). The forward dynamics are driven by the activation levels of each muscle, which computes a muscle's net force using a Hill-based muscle model (Section 3.3). See Appendix A for the anatomy of the human hand and arm.

3.1 Rigid Bodies and Joints

Using the geometric model of the left hand from the Ultimate Human model, which was provided by Sung-Hee Lee, we extracted geometric models of each bone in the hand. In our simulation of the hand and forearm, all bones are passive rigid bodies with the assumption that bone deformations within the hand are not possible. There are a total of 16 passive rigid bodies that comprise 30 bones. For simplicity, the position and orientation of the ulna and radius (which are grouped together as one rigid body) are fixed, making it impossible to perform supination/pronation. Thus, the forearm rigid body does not move and the hand is free to produce different hand motions and gestures. The rigid body representing the palm consists of the 8 carpals, 5 metacarpals and the sesamoid bone. The remaining rigid bodies are the individual bones for the phalanges.

The system contains a total of 16 degrees of freedom (DoFs). The thumb comprises 2 bones (the 1st proximal phalanx and the 1st distal phalanx) and 2 single axis joints (a total of 2 DoFs). The other four fingers are made up of 3 bones (the proximal phalanx, the intermediate phalanx, and the distal phalanx) and each finger has 3 single axis joints (a total of 12 DoFs). There are single axis joints connecting the metacarpals to the proximal phalanges and another connecting the phalanges to one another. The wrist contains a double axis joint that connects the palm and forearm (a total of 2 DoFs). The single axis joint is modeled as a hinge joint, which has one DoF, and the double axis joint is modeled as a universal joint with two DoFs. OpenSceneGraph (Section 4.2) is used to set the tree hierarchy of the bones along with their visualization. The Open Dynamics Engine (Section 4.1) is used to organize and run the dynamics of the simulation.

3.2 Muscle Model

There are a total of 25 muscles within the hand and forearm model. There are 3 muscles for the thumb, 4 muscles for each finger, and 6 muscles for the wrist. Due to the simplifications of the forearm and the palm, muscles that are used for grasping, abduction, adduction, supination and pronation were not modeled (with the exception of abduction and adduction for the wrist).

A biological muscle's contractile force is directly proportional to its cross-section and length. Since we model muscles as massless B-splines, the cross-section of the muscle does not play a role in computing the contractile force generated by each muscle. The length of the muscle is the primary variable that determines the amount of contractile forces generated by each muscle.

3.2.1 B–Spline Representation

Sueda et al. (2008) represented each muscle with a B-spline strand that interpolates along a series of constraint points. The B-splines in this simulation are used only for visualizing the muscle and managing its length. Unlike interpolating B-spline strands, the approximating uniform cubic B-splines are used to route the muscles along the bones. Since these are massless approximating splines, they have no dynamic properties (e.g., mass, velocity, etc) and according to the definition of a strand in (Sueda et al., 2008), are not considered to be strands. Since our muscle model lacks dynamic properties, we do not model the momentum of the muscle.

By using cubic B-splines, a minimum of 4 control points are needed to create a single spline. Each muscle has m control points, where $m \geq 4$ and is an arbitrary number that varies for each muscle.

The following blending function is used to compute the uniform cubic B-spline for one uniform knot-interval:

$$S_i(t) = \begin{bmatrix} t^3 & t^2 & t & 1 \end{bmatrix} \frac{1}{6} \begin{bmatrix} -1 & 3 & -3 & 1 \\ 3 & -6 & 3 & 0 \\ -3 & 0 & 3 & 0 \\ 1 & 4 & 1 & 0 \end{bmatrix} \begin{bmatrix} P_i \\ P_{i+1} \\ P_{i+2} \\ P_{i+3} \end{bmatrix}. \tag{3.1}$$

In this blending function, P_i are the coordinates of the i^{th} control point. To create the entire spline of the muscle, S_i is computed starting from $i = 0$ to $i = m-4$. In each knot interval, the spline is drawn using a cylinder at increments of $t = 0.1$, for $t \in [0, 1]$. Computing all of the $S_i(t)$ intervals yields a spline that represents a single muscle.

To make it possible for a muscle to apply force, the muscle needs to connect to the bone. As a result, a simple feature of making the splines interpolate at the end points of the muscle (the first and last points in the set of control points) was added. To do this, two extra spline knot intervals are inserted into the spline computing process for each end point of the spline.

For the first endpoint, before S_0 is computed, two special spline computations are included. The first is a blending function with the control points as $[P_0\ P_0\ P_0\ P_1]^T$, and the second with the control points as $[P_0\ P_0\ P_1\ P_2]^T$. After these two special computations are made, S_i is computed.

For the last endpoint, after S_{m-4} is computed, two special spline computations are added. The first has the control points as $[P_{m-3}\ P_{m-2}\ P_{m-1}\ P_{m-1}]^T$, and the second has the control points as $[P_{m-2}\ P_{m-1}\ P_{m-1}\ P_{m-1}]^T$.

These extra spline computations allow the spline to interpolate the two end points. This is not a method that is normally used, but it serves the purpose of interpolating the end points, while not causing any major effects on the muscle spline itself. Given the interpolation, the spline attaches exactly at the points of insertion where it is attached to the bone. With these insertion points, spline tangents are computed and used to calculate the direction at which to apply torques to the bones.

3.2.2 B–Spline Control Points

Using the Ultimate Human model as a guide, the geometric models of the muscles are used to approximate the control points of each muscle spline. With the help of the open source 3D viewing program Blender (`http://www.blender.org`), every control point was manually chosen along the muscle fibers to keep consistent with the shape and structure of each muscle. Our muscle routings attempt to follow the realistic routings of the muscle as closely as possible. See Appendix C for sets of all muscle control points.

3.3 Forward Dynamics Simulation

3.3.1 Hill–Based Muscle Model

A Hill-based muscle model is used for each muscle actuator. Our simulation employs a simplified version of the three-element Hill-based model described by Ng-Thow-Hing (2001). The described model includes a series element (SE), a parallel element (PE), and a contractile element (CE). Since each muscle is modeled as a spline, no series elements are present in our simulation. Thus, the muscle model is only concerned with the PE and CE, similar to that of Lee and Terzopoulos (2006).

The PE represents the passive elastic properties of the muscles, and produces a restoring force:

$$f_P = \max(0, k_s \exp(k_c e) - 1 + k_d \dot{e}), \tag{3.2}$$

where k_s and k_c are the muscle elastic coeficients, k_d is the damping coefficient, $e = (l - l_0)/l_0$ is the muscle strain, and $\dot{e} = \dot{l}/l_0$ is the muscle strain rate, with l and l_0 representing the muscles length and slack length, respectively.

The CE represents the source of active force generation and produces a contractile force $f_C = aF_l(l)F_v(\dot{l})$ that is dependent on the muscle activation a, the force-length relation,

$$F_l = \max(0, k_{\max}(l - l_m)), \tag{3.3}$$

and the force-velocity-relation,

$$F_v(\dot{l}) = \max(0, 1 + \min(1 + \min(\dot{l}, 0)/v_m)), \tag{3.4}$$

where $k_{\max}$ is the maximum stiffness of the muscle when it is fully activated, l_m is the minimum length at which the muscle can produce force, and v_m is the maximum contraction velocity under no load. We set the $l_m = 0.5l_0$ and $v_m = 8l_0$ sec^{-1} per (Lee and Terzopoulos, 2006).

3.3.2 Manual Activations

Described by the Hill-based muscle model in the previous section, the muscle's activation controls the net force generated by each muscle. Each muscle has a linear activation level, where 0 indicates no activation and 1 is full activation. The activation level is similar to the percentage that a muscle contracts. As the muscle contracts, pulling forces are produced that apply torques on the rigid bodies. While the simulation runs, users can manually increase or decrease the activation of each muscle, allowing the demonstration of a range of possible hand motions.

CHAPTER 4

Implementation

Our simulation was implemented in C++ and built on top of two open source toolkits: Open Dynamics Engine (Section 4.1) and OpenSceneGraph (Section 4.2)

4.1 Open Dynamics Engine

Open Dynamics Engine (ODE) (Toolan, 2006) is a physics engine designed for real-time dynamics simulations. ODE is used to simulate the dynamics of articulated rigid bodies in our system. ODE has a large array of built-in functions that are particularly useful for generating the dynamics environment, in which rigid bodies are created and placed within this dynamics world. By using ODE's joint models, the hierarchy of the articulated hand model was created. For the dynamics of each bone, detailed properties of each bone's mass, inertia tensors, positions, and axes of rotation were computed from the geometry of the Ultimate Human model. Due to the simplifications in the system, object collision is not possible. Hence, collisions are not taken into account, but the implementation of collisions can easily be implemented with ODE's collision detection classes. ODE has an integrator that is very stable and will accurately simulate the system as long as step sizes are small. The simulation uses a fixed timestep of 0.041667 sec (or 24 frames per second).

4.2 OpenSceneGraph

OpenScenegraph (OSG) is a graphics toolkit that is used for the visualization of the simulation. Like ODE, OSG has many functions and classes that allowed us to set up the simulation. Using OSG's API, the geometry (from the Ultimate Human model) for our hand model was loaded and the articulated object hierarchy for the scene graph data structure was created.

4.2.1 Rigid Bodies

OpenSceneGraph has a built-in mechanism to build matrix transformation hierarchies by creating the appropriate directed acyclic graph (DAG) with its *MatrixTransform* nodes. By extending this mechanism to save a rigid body's state, the *RigidBodyTransform* node was created. A *RigidBodyTransform* node, therefore, encapsulates the matrix transformation hierarchy and the rigid body properties to properly display and simulate the bones of our hand model. Each bone is set as a child of a *RigidBodyTransform*.

4.2.2 Joints

To incorporate the joint constraints modeled by ODE, the *HingeJointGroup* node and the *UniversalJointGroup* node were created. Both of these nodes can parent up to two *RigidBodyTransform* nodes. If only one rigid body is specified, the joint will fix the position of the specified rigid body to ODE's static environment, fixing the orientation and position of the specified rigid body. If two rigid bodies are specified, the joint will be attached to both rigid bodies. A *HingeJointGroup* node has the same properties of a hinge joint: the rigid bodies it is attached to, its position, its axis of rotation, its low stop angle, and its high stop angle. The

UniversalJointGroup has the same properties of a hinge joint, but with an extra axis and an additional low/ high stop angle for this extra axis.

4.2.3 Muscle Control Points

The set of control points for the muscles were picked when the rigid bodies were at their initial position. However, since the rigid bodies move, the control points must also move along with the rigid body. To solve this problem, each control point is a child of a bone in the scene graph. All affine transformations of the bone are propagated to its children control points, allowing the control points to move along with the bone. After every time-step of the simulation, the muscle spline will update its set of control points. With every update, the drawn muscle spline will appear to move along with the bone. As this occurs, the length of each muscle is constantly updated, which allows us to compute new forces generated by each muscle after every time-step. Since control points move along with the bones, spline intersections with the bone may occur. This was minimized by choosing control points that will not intersect with one another or the bone as they move. See Appendix C for the muscle control points along with the rigid body that they parent.

4.2.4 Node Callbacks

By utilizing OSG's *NodeCallback* mechanism, our simulator is able to incorporate the dynamics simulation with the visualization. A *RigidBodyCallback* class was created to interject the ODE simulation into the scene graph. The *RigidBodyCallback* class is responsible for updating the positions and orientations of each bone based on the ODE rigid body dynamics simulation. More specifically, the *RigidBodyCallback* class takes the updated positions and orientations of the rigid bodies in ODE and updates each matrix transformation within each bone's *RigidBodyTransform* node.

To transmit the muscle forces to the bones, a *SplineGeodeCallback* class was created. In OSG, a *Geode* is just a node within the scene graph that contains geometric data. The *SplineGeodeCallback* class updates the geometry of the muscle splines by recomputing the positions of the splines' control points. The *SplineGeodeCallback* is also responsible for computing and transmitting the contractile and restoring forces computed by the Hill-based muscle model.

Starting, stopping and resetting the ODE simulation is handled by the *SimulationCallback* class. This callback simply advances ODE's integration step by the specified step size, which in our simulation is equal to 0.041667 sec, yielding 24 frames per second.

CHAPTER 5

Simulation Results and Analysis

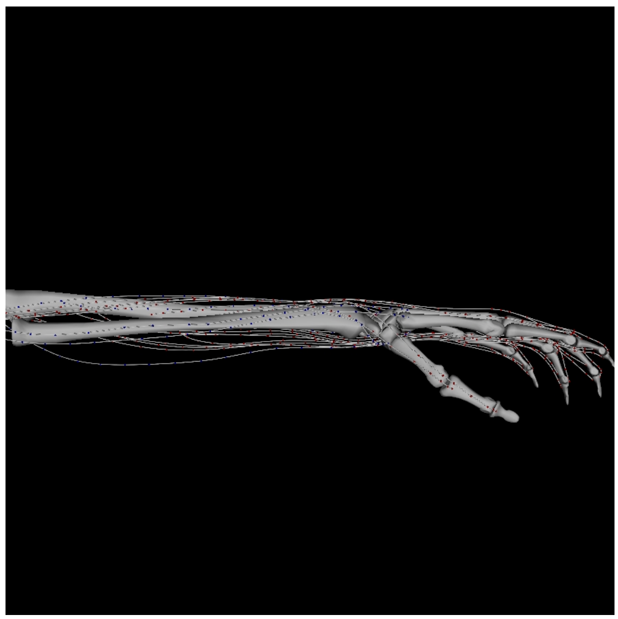

Figure 5.1: Rest pose

In our model of the human hand, there are a total of 25 muscles splines and 16 bone rigid bodies. For simplicity, 14 bones in the palm (along with the sesamoid bone) were combined into one rigid body, and the ulna and radius into another. With this design, 19 muscle splines are used to control the movement of the fingers and 6 muscle splines control movement of the wrist. Our simulator is able to implement a forward dynamics simulation for the flexion/extension of each finger and flexion/extension/abduction/adduction for the wrist. Figure 5.1 shows the rest pose of the simulated hand.

5.1 Thumb

The thumb is made up of 2 bones and 3 muscles. Muscles mla007 and mla008 run along the top of the thumb, and muscle mla013 runs along the bottom of the thumb. mla007 and mla013 are both attached to the thumb's distal phalanx, while mla008 is attached to the thumb's proximal phalanx. Figure 5.2(a) shows the thumb flexed and Figure 5.2(b) shows the thumb fully extended. Table 5.1 shows the different muscle lengths in 3 distinct poses: fully flexed, at rest, and fully extended.

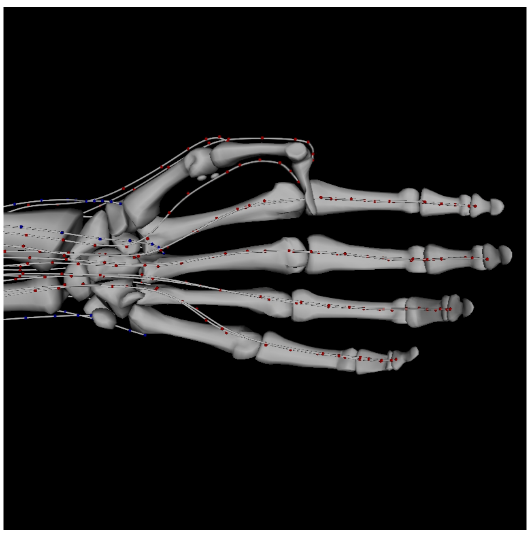

(a) Flexion

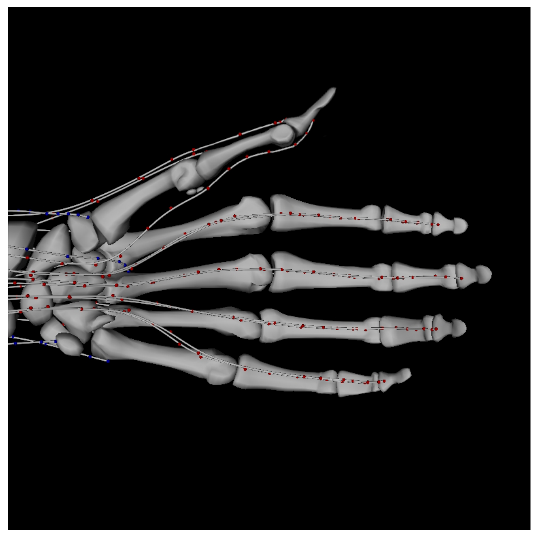

(b) Extension

Figure 5.2: Flexion/Extension of the thumb

Muscle	Fully Flexed	At Rest	Fully Extended
mla007	313.428154	308.099939	305.328347
mla008	213.224231	209.334723	205.830832
mla013	355.817232	360.915243	364.318294

Table 5.1: Thumb muscle lengths at different poses

5.2 Index Finger

The index finger is made up of 3 bones and 4 muscles. Muscles mla005k and mla005r run along the top of the index finger. Muscles mla011d and mla012l run along the bottom of the index finger. mla005k and mla011d are attached to the index finger's distal phalanx, while mla005r and mla012l are attached to the index finger's intermediate phalanx. Figure 5.3(a) shows the index finger fully flexed and Figure 5.3(b) shows the index finger fully extended. Table 5.2 shows the different muscle lengths in 3 distinct poses: fully flexed, at rest, and fully extended.

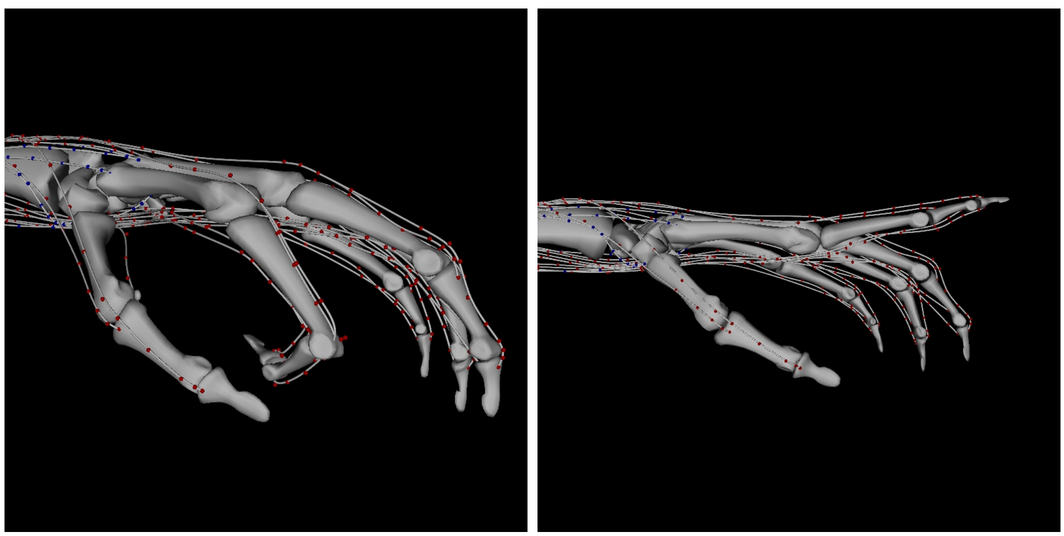

(a) Flexion

(b) Extension

Figure 5.3: Flexion/Extension of the index finger

Muscle	Fully Flexed	At Rest	Fully Extended
mla005k	522.524171	514.961266	509.188157
mla005r	494.513887	487.930814	483.727941
mla011d	386.300041	416.269679	423.083044
mla012l	311.656180	334.696352	339.272562

Table 5.2: Index finger muscle lengths at different poses

5.3 Middle Finger

The middle finger is made up of 3 bones and 4 muscles. Muscles mla005c and mla005g run along the top of the middle finger. Muscles mla011a and mla012a run along the bottom of the finger. mla005c and mla011a are attached to the middle finger's distal phalanx, while mla005g and mla012a are attached to the middle finger's intermediate phalanx. Figure 5.4(a) shows the middle finger fully flexed and Figure 5.4(b) shows the middle finger fully extended. Table 5.3 shows the different muscle lengths in 3 distinct poses: fully flexed, at rest, and fully extended.

Muscle	Fully Flexed	At Rest	Fully Extended
mla005c	520.330351	504.662531	497.232866
mla005g	482.005509	470.747805	464.964399
mla011a	423.063614	447.768248	460.991492
mla012a	371.916996	392.363353	403.403514

Table 5.3: Middle finger muscle lengths at different poses

5.4 Ring Finger

The ring finger is made up of 3 bones and 4 muscles. Muscles mla005n and mla005p run along the top of the ring finger. Muscles mla011c and mla012k run along the bottom of the finger. mla005n and mla011c are attached to the ring finger's distal phalanx, while mla005p and mla012k are attached to the ring finger's intermediate phalanx. Figure 5.5(a) shows the ring finger fully flexed and

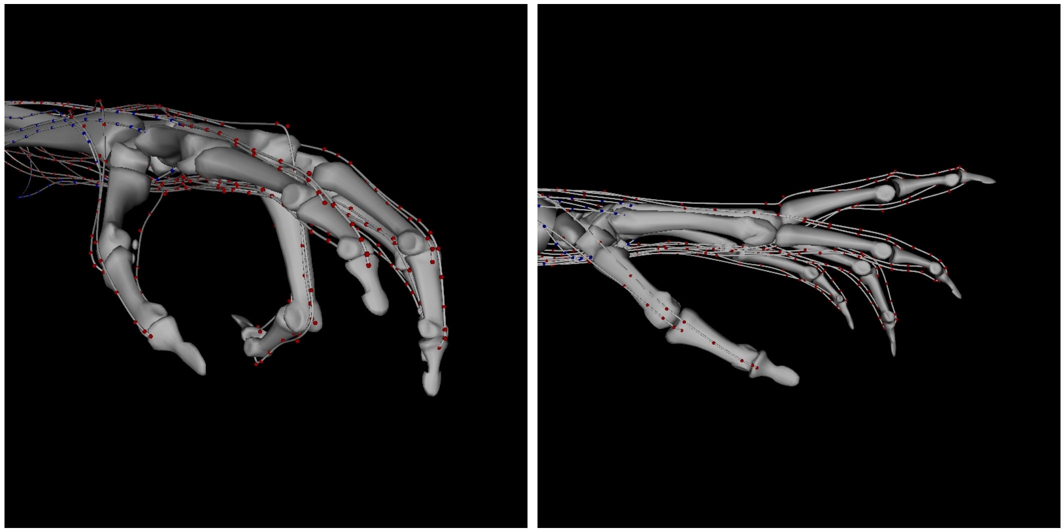

(a) Flexion (b) Extension

Figure 5.4: Flexion/Extension of the middle finger

Figure 5.5(b) shows the ring finger fully extended. Table 5.4 shows the different muscle lengths in 3 distinct poses: fully flexed, at rest, and fully extended.

Muscle	**Fully Flexed**	**At Rest**	**Fully Extended**
mla005n	509.027328	500.044760	493.918862
mla005p	476.320969	469.285095	464.424669
mla011c	369.550311	388.046624	397.306861
mla012k	442.014393	454.244883	463.911767

Table 5.4: Ring finger muscle lengths at different poses

5.5 Little Finger

The little finger is made up of 3 bones and 4 muscles. Muscles mha007c and mha007a run along the top of the little finger. Muscles mla011b and mla012u run along the bottom of the finger. mha007c and mla011b are attached to the little finger's distal phalanx, while mha007a and mla012u are attached to the little

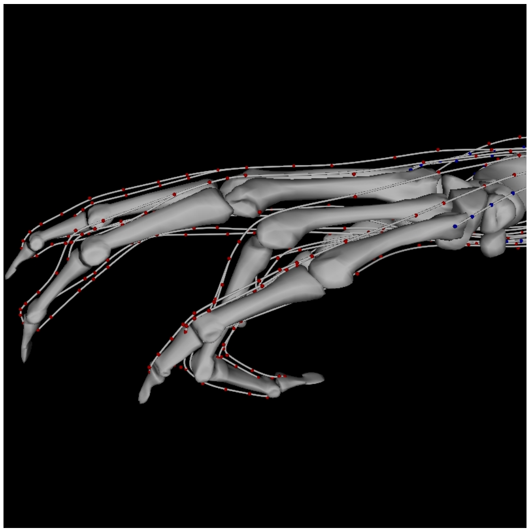

(a) Flexion

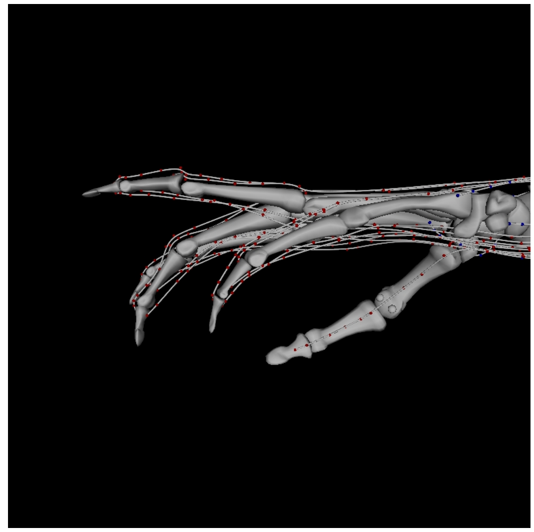

(b) Extension

Figure 5.5: Flexion/Extension of the ring finger

finger's intermediate phalanx. Figure 5.6(a) shows the little finger fully flexed and Figure 5.6(b) shows the little finger fully extended. Table 5.5 shows the different muscle lengths in 3 distinct poses: fully flexed, rest, and fully extended.

Muscle	Fully Flexed	At Rest	Fully Extended
mha007c	481.442920	467.589788	462.928727
mha007a	458.264327	446.556490	442.924211
mla011b	317.490473	331.566456	338.764605
mla012u	450.595156	461.338340	467.895771

Table 5.5: Little finger muscle lengths at different poses

5.6 Wrist

The wrist consists of 2 rigid bodies (palm rigid body which has 14 bones and the forearm rigid body, which has 2 bones) and 6 muscles splines. All of the muscles are attached to the palm rigid body. Figure 5.7 depicts the attachments. Muscle

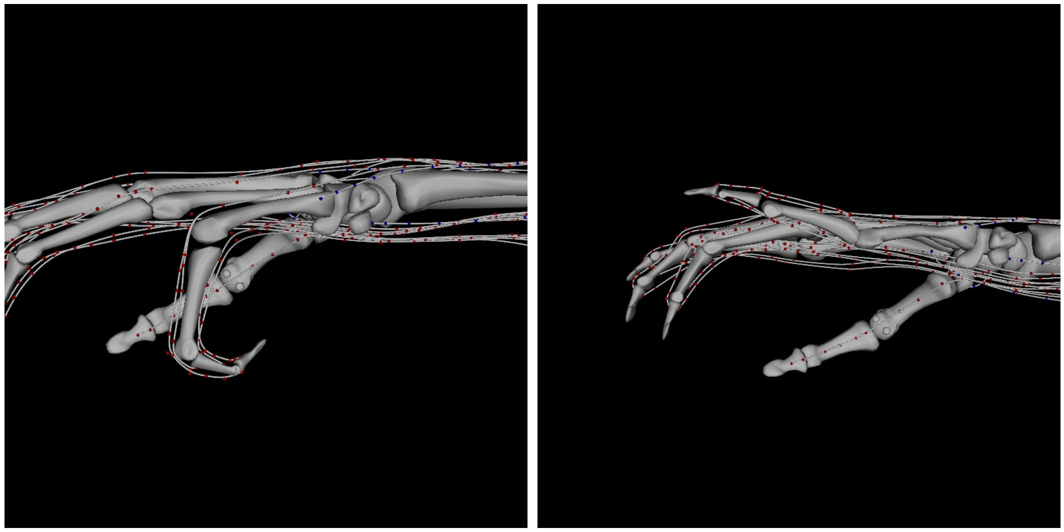

(a) Flexion (b) Extension

Figure 5.6: Flexion/Extension of the little finger

mla002 is attached at (A). Muscle mla004 is attached at (D). Muscle mla003 is attached at (B). Muscle mha003 is attached at (C). Muscle mla008 is attached at (E). Muscle mla010 is attached at (F).

Muscle	**Fully Flexed**	**Fully Extended**	**At Rest**	**Abduction**	**Adduction**
mla002	343.670898	327.408081	336.214140	341.432820	339.131573
mha003	266.060788	272.086907	270.005433	263.069013	282.506919
mla003	389.088774	378.175849	384.657201	387.678975	389.551420
mla004	352.301125	337.426388	344.995824	352.964430	343.533354
mla008	367.213934	381.504770	375.268552	373.158725	376.503562
mla010	305.500122	310.819099	308.048770	309.738591	309.455478

Table 5.6: Wrist muscle lengths at different poses

Figure 5.8(a) shows the wrist performing flexion and Figure 5.8(b) shows the wrist performing extension. Figure 5.8(c) shows the wrist performing abduction and Figure 5.8(d) shows the wrist performing adduction. Table 5.6 shows the different muscle lengths in 5 distinct poses: fully flexed, fully extended, at rest, abduction and adduction.

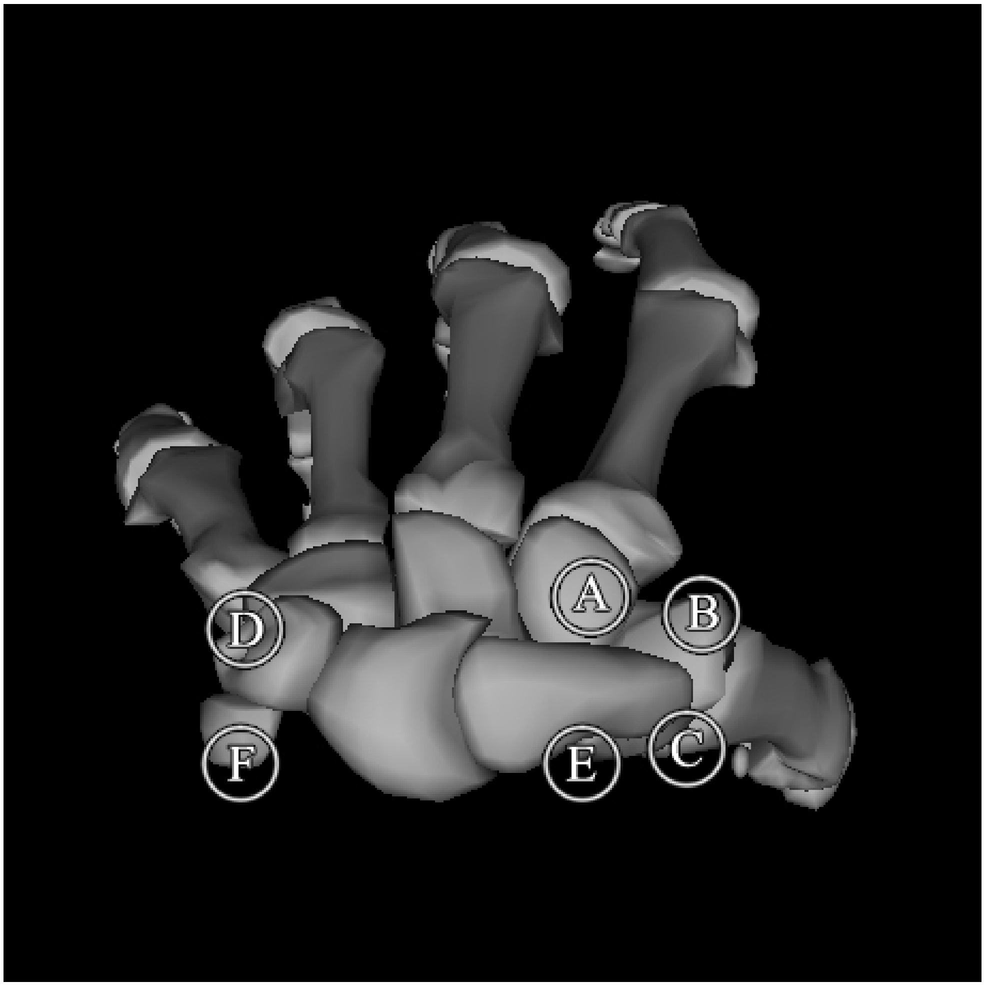

Figure 5.7: Wrist muscle attachments

5.7 Analysis

From the results, we observed that the fingers were able to achieve the poses of flexed and extended while the wrist achieved the poses of flexed, extended, abducted, and adducted. These poses are achieved by giving each muscle certain activation levels. Since each muscle is attached to a bone, the muscle applies forces at their bone insertion points in accordance with the specified activation levels. Every finger has two muscles running along the top and two along bottom;

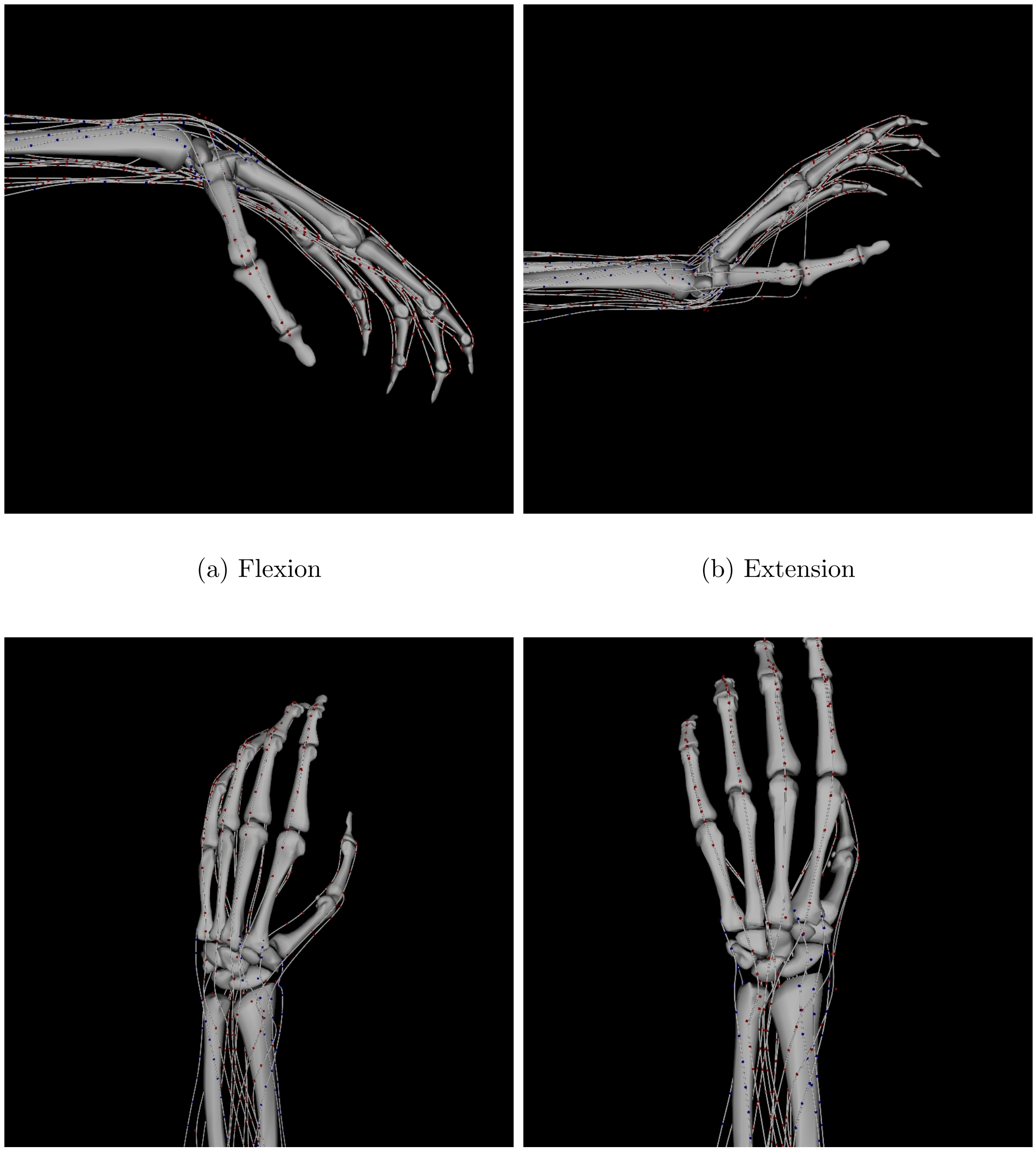

(a) Flexion (b) Extension

(c) Abduction (d) Adduction

Figure 5.8: Flexion/Extension/Abduction/Adduction of the wrist

while the thumb has only one muscle running along the bottom. This muscle configuration for the fingers allows the fingers to perform flexing and extending. Fingers are capable of abducting and adducting, but the muscles required for this range of motion are not simulated. The wrist has six muscle attachments, inserted all around the wrist, allowing it to flex, extend, abduct, and adduct. The wrist is capable of supination and pronation but the muscles and bones required for this range of motion are not simulated.

The above figures display the poses achieved by the fingers and wrist. In each pose, certain muscles are contracted while the others are stretched, particularly those opposing the contracted muscles. When a finger is flexed, it is evident that the bottom two muscles are contracted and the top two are stretched. When a finger is extended, the top two muscles are contracted and the bottom two are stretched. The same concept of contraction and stretching applies to the wrist for each pose that is achieved. As is indicated in the above tables for each pose, contraction is represented by shorter muscle lengths and stretching by longer muscle lengths. The muscle length in the rest pose is the initial starting length from when the simulation starts, which is between the flexed and extended poses.

It should be noted that the poses are not considered to be fully flexed, fully extended, fully abducted, or fully adducted. Only a certain level of flexing and extension can be achieved in the simulation. Abduction and adduction from the wrist was imperfect. Despite the motions not being done in full and perfectly, the figures in the results depict poses that are achievable to the best of our simulator's abilities. The results show that the simulation is capable of producing these basic hand motions despite its simplifications.

The data in the tables indicate that the motions of the fingers and wrist require certain sets of muscles to contract. Therefore, in order to produce different poses for each finger and wrist, different combinations of muscles must be given different activation levels. By setting certain activation levels to different combinations of muscles, different hand motions involving all of the fingers can be achieved through our forward dynamics simulation.

Just like a real human's hand, particular combinations of muscles are required to produce certain hand motions. The results of the simulation reveal the sets of muscles that are used for each of the displayed poses, along with how much effort each muscle must make to produce the hand gesture, which is determined by the muscle lengths of the pose results.

CHAPTER 6

Conclusion

This thesis presented a biomechanical simulator of the human hand and forearm. Modeling the bones as rigid bodies and the muscles as splines, we were able to simulate a large range of hand motions with the use of forward dynamics. Our biomechanical model closely resembles that of a real human's left hand. By using anatomically accurate geometrical models and closely following the complex routing of muscles, our model resembles a real human hand. The results of this study are valuable for computer animation and potentially also for biomechanics.

Aside from the Ultimate Human model geometric data, our simulator was implemented using open source toolkits. Despite the simplifications made in the modeling, our simulations were able to achieve the goal of producing different realistic hand gestures through forward dynamics. Our results further support the idea that forward dynamics is a viable approach used for character animations in place of inverse kinematics.

In terms of biomechanics, the musculoskeletal model in this simulator is unique as it is a realistic modeling of the human hand. Due to the hand's intrinsic and complex muscle routings, the model in our simulation provides valuable information regarding how the dynamics of the human hand works. The model provides detailed information about how the human hand's muscles work together to perform certain tasks. As in (Lee et al., 2009), such models can provide valuable information in how the human body functions.

6.1 Future Work

Although our simulator is capable of producing a large range of basic hand motions driven by forward dynamics, there are many areas in which the simulation can be further improved.

The performance of our simulator greatly depends on the detailed modeling of the human hand, particularly the musculoskeletal model in the simulation. Our current model cannot perform abduction/adduction of the fingers and supination/pronation of the wrist. By simulating additional muscles and bones, our simulator can be made capable of producing a larger variety of motions. This would prove to be very valuable, as adding new musculoskeletal components into our simulator would greatly increase the number of simulated degrees of freedom and, consequently, allow the simulation to produce more realistic hand motions, such as grasping, gripping, and waving.

Another area that requires further work is the way muscle activations are handled. The simulation currently requires manual activation of all muscles in order to produce hand motions, which is tedious. Due to the positioning of the muscle attachments to each bone, certain muscles produce greater torque than other muscles with the same activation level. An automated muscle activation controller would obviate this manual muscle activation process.

Very few studies have been done on accurately modeling human bodies, one of them being (Lee et al., 2009), but it did not include a biomechanical model of the hand, a limitation that our hand model and simulator can help overcome with additional research. Finally, adding dynamics to the muscles would greatly increase the realism of human body simulation. Although Sueda et al. (2008) have implemented muscles as dynamic strands, our simulation employs muscle routings that are mapped directly from a realistic model of a human. With this realistic mapping of muscles, the addition of dynamics to the muscles would provide great insight on the biomechanical basis of human hand motions.

APPENDIX A

Anatomy

A.1 Bones

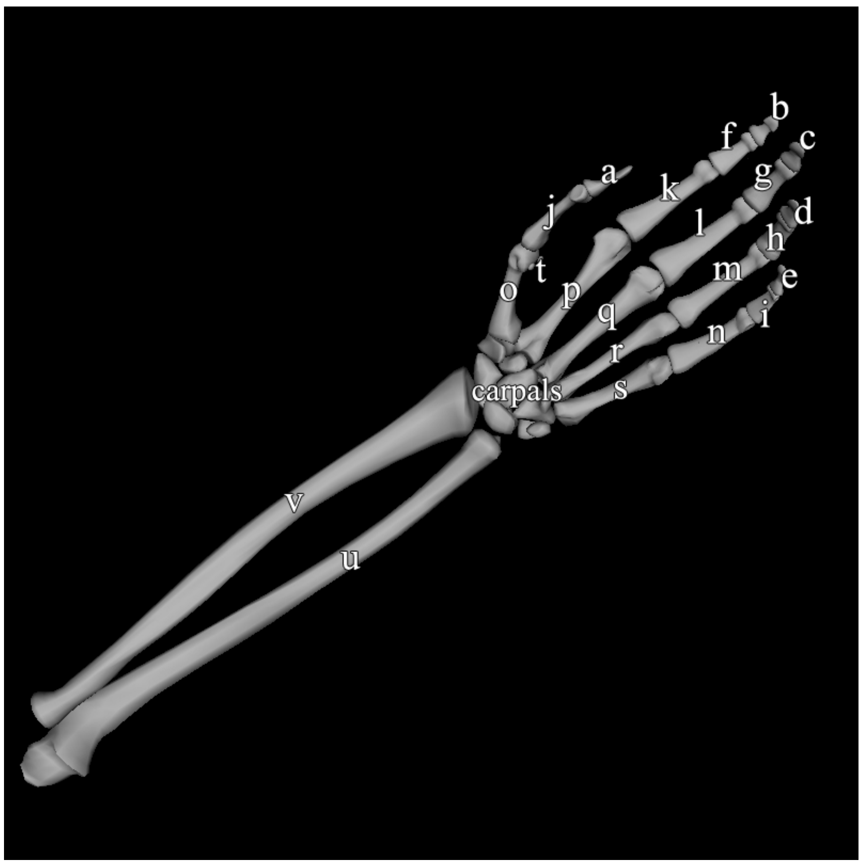

Figure A.1: **Skeletal structure of the human hand and forearm**
a-e: distal phalanges; f-i: intermediate phalanges; j-n: proximal phalanges; o-s: metacarpals; t: sesamoid bone; u: radius; v: ulna. There are 8 carpal bones in the palm.

A.2 Bones and Muscles from the Ultimate Human Model

(a) No Muscles

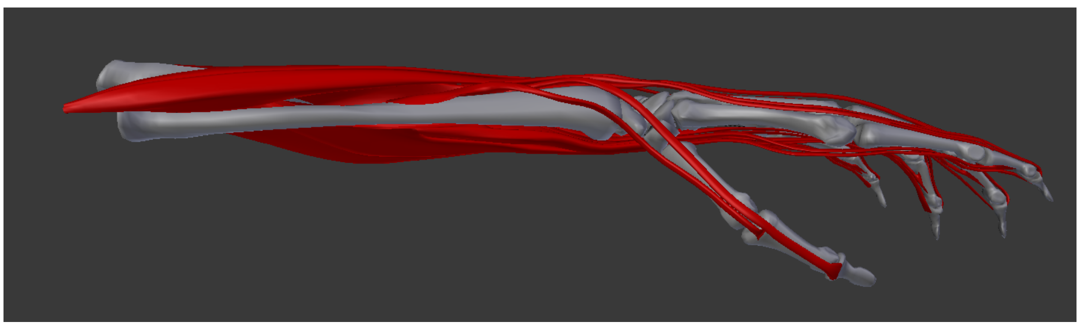

(b) Hand Muscles

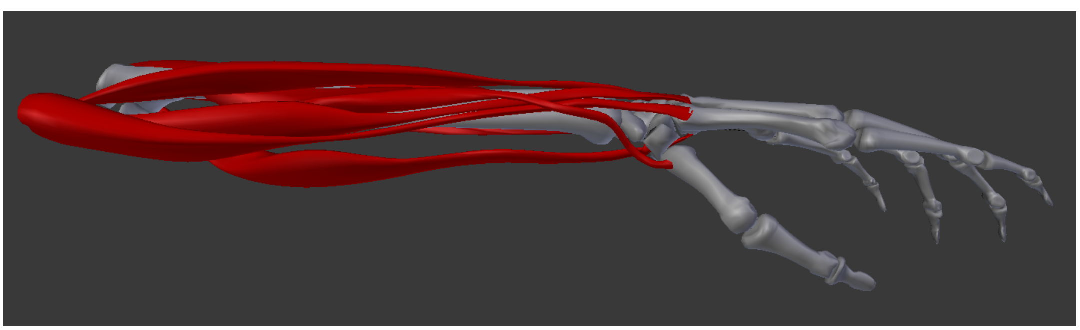

(c) Wrist Muscles

Figure A.2: Right lateral view of the hand

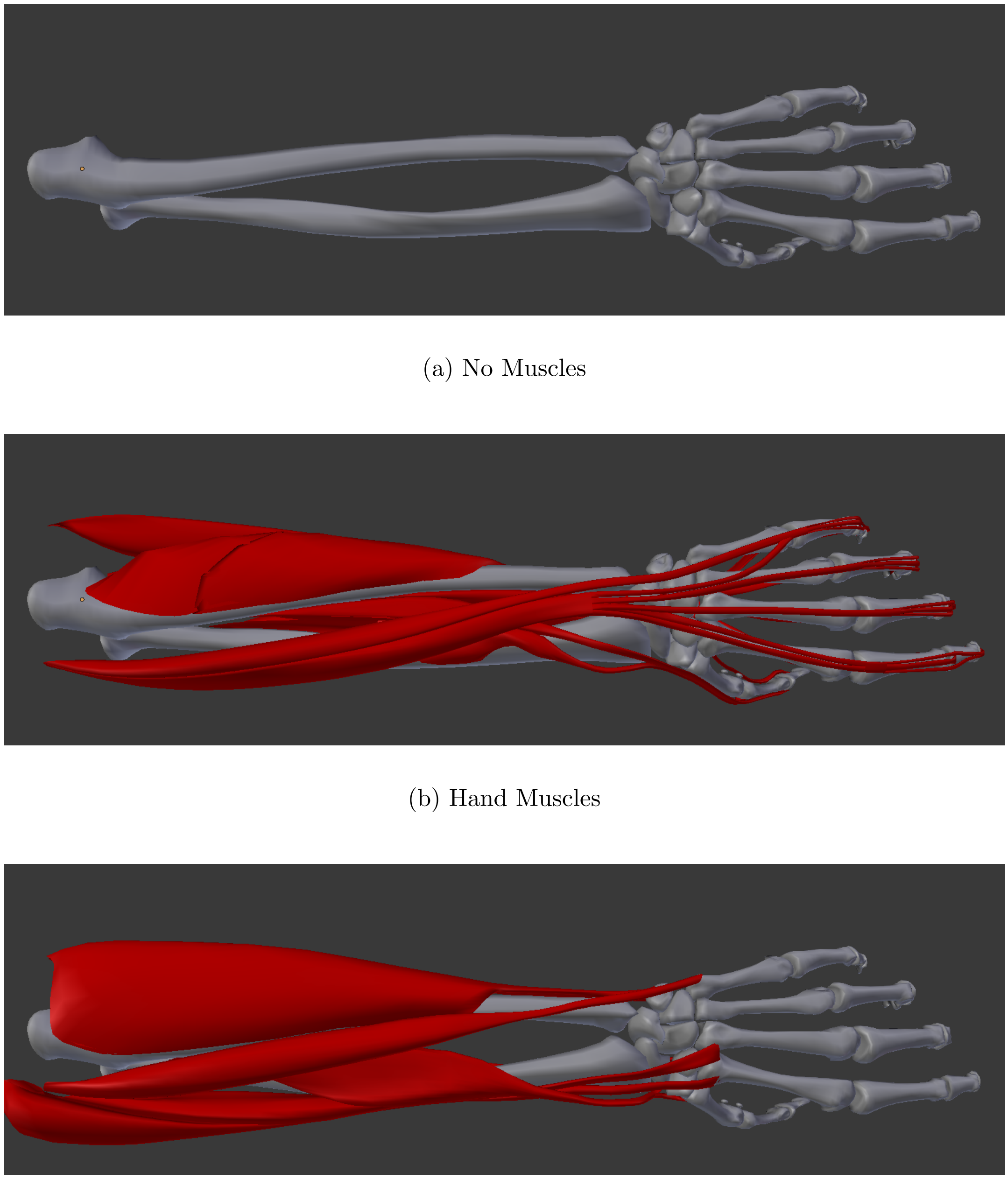

(a) No Muscles

(b) Hand Muscles

(c) Wrist Muscles

Figure A.3: Top view of the hand

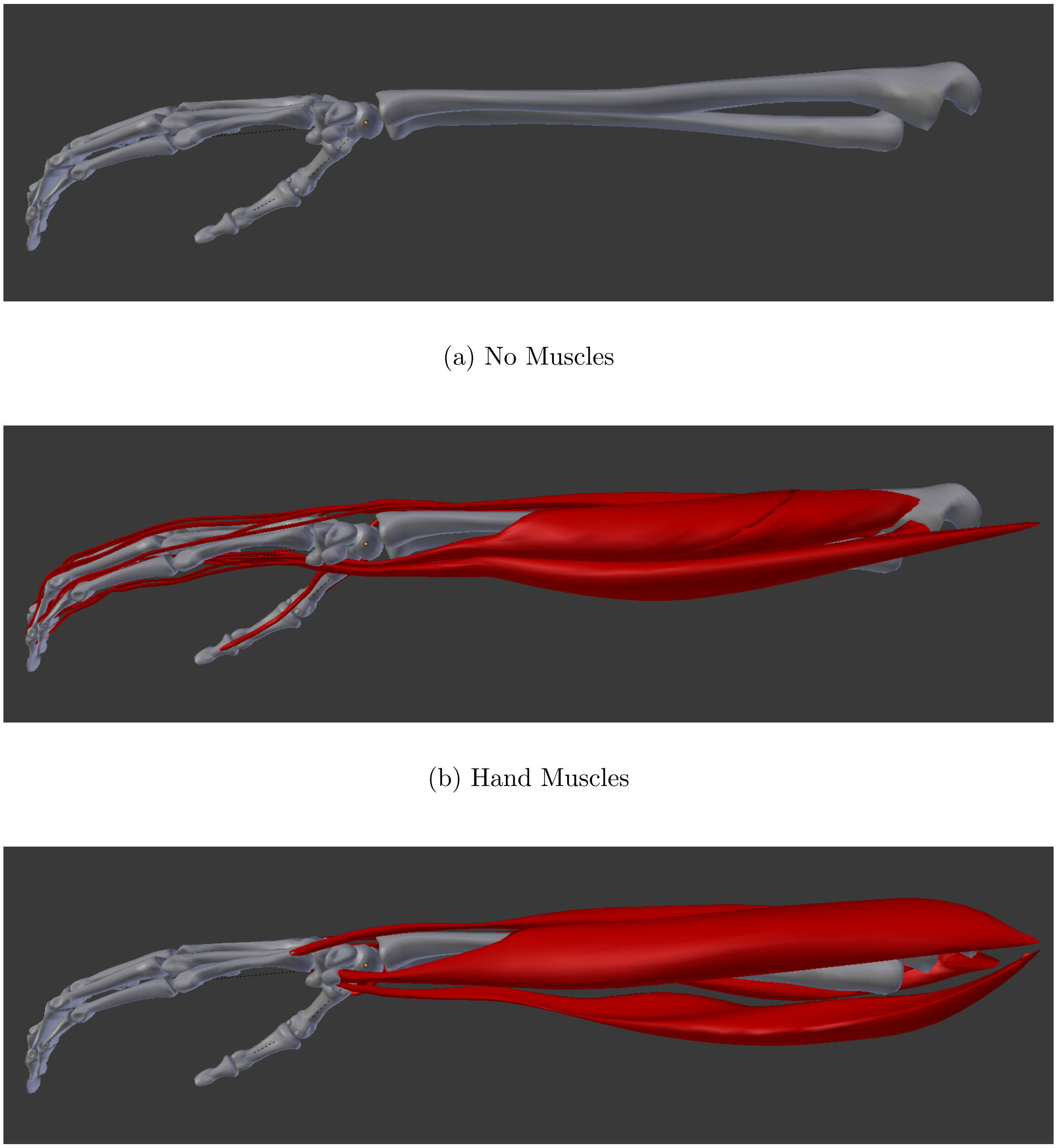

(a) No Muscles

(b) Hand Muscles

(c) Wrist Muscles

Figure A.4: Left lateral view of the hand

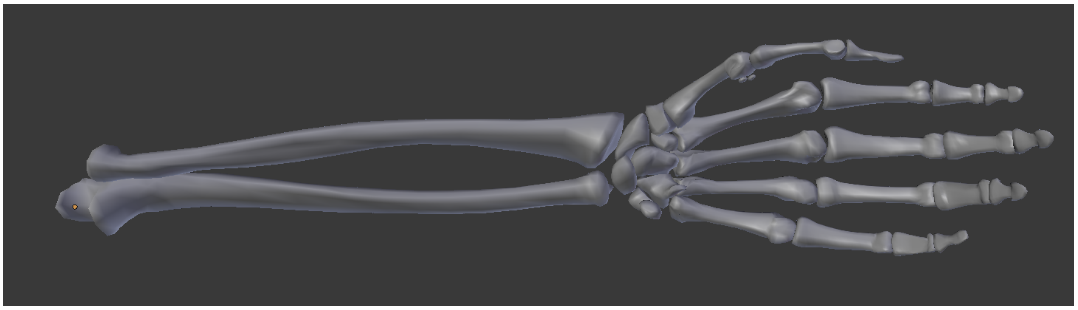

(a) No Muscles

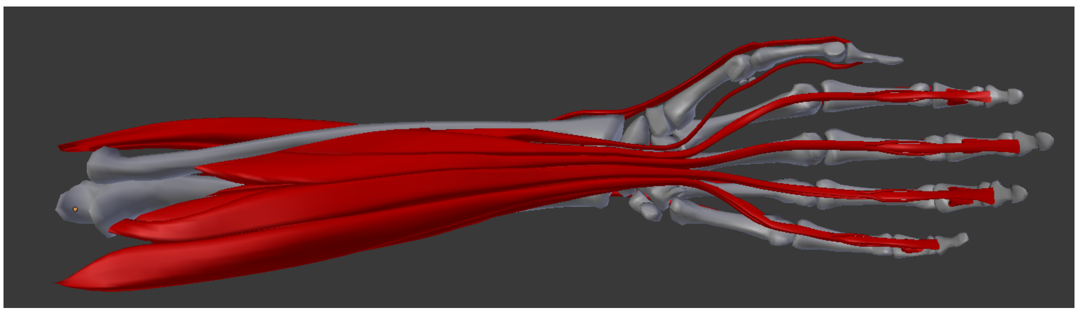

(b) Hand Muscles

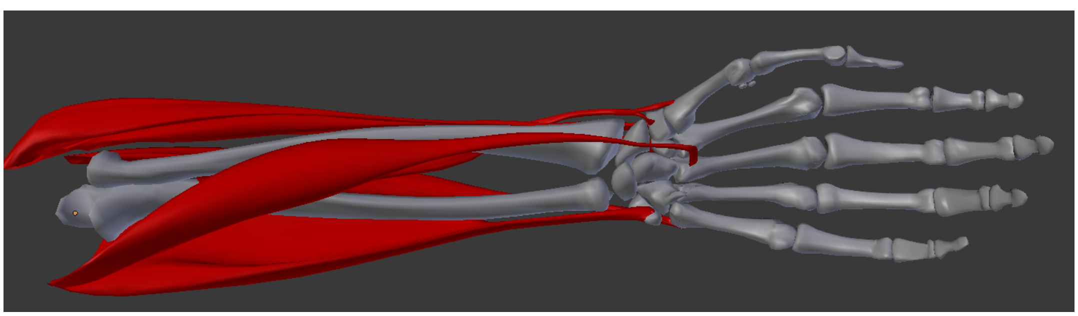

(c) Wrist Muscles

Figure A.5: Bottom view of the hand

A.3 Muscles

A.3.1 List of Muscles

Muscle Group	#	Muscle Name	Inserts Into
Hand	1c	mla005c	Middle Finger
	1g	mla005g	
	1k	mla005k	Index Finger
	1n	mla005n	Ring Finger
	1p	mla005p	
	1r	mla005r	Index Finger
	2	mla006	Thumb
	3a	mha007a	Little Finger
	3c	mha007c	
	4	mla007	Thumb
	5	mla008	
	6a	mla011a	Middle Finger
	6b	mla011b	Little Finger
	6c	mla011c	Ring Finger
	6d	mla011d	Index Finger
	7a	mla012a	Middle Finger
	7k	mla012k	Ring Finger
	7l	mla012l	Index Finger
	7u	mla012u	Little Finger
	8	mla013	Thumb
Wrist	9	mla002	Wrist
	10	mha003	
	11	mla003	
	12	mla004	
	13	mla008	
	14	mla010	

Table A.1: **Muscle groups and names**
Note: *There are 25 muscles modeled in our simulator. mla006 is listed but not simulated.*

A.3.2 Hand Muscles

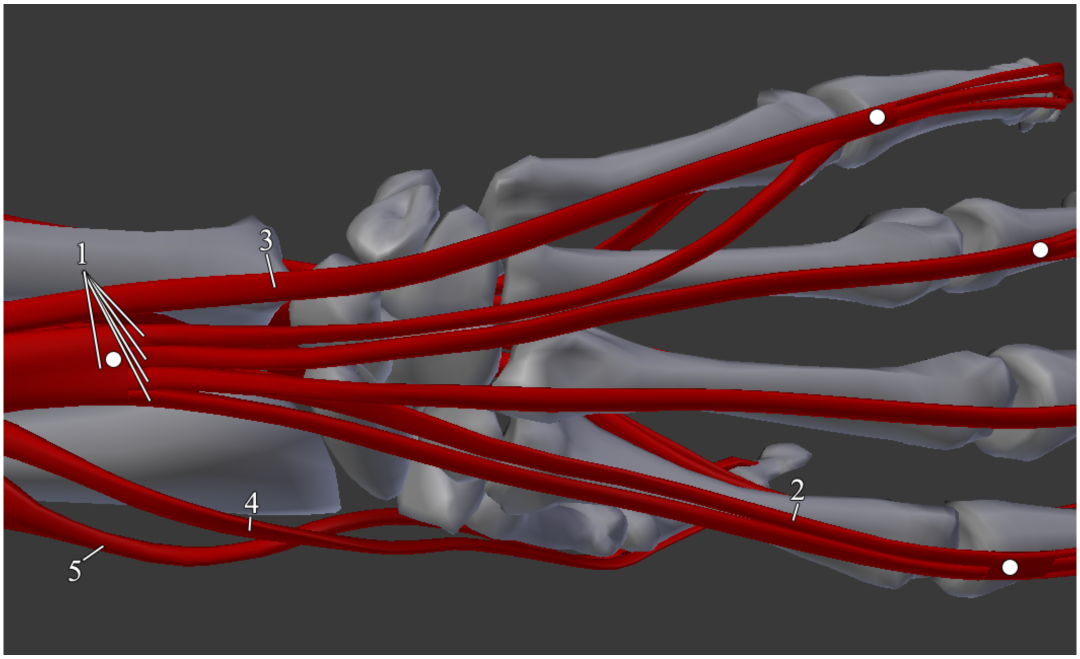

Figure A.6: **Hand upper muscles**
(1) mla005, **(2)** mla006, **(3)** mha007, **(4)** mla007, **(5)** mla008, **(•)** Muscle splits into smaller strands

Muscles mla005 splits from one large muscle into four smaller muscle strands, and then splits again into smaller muscle strands before they are attached to the bones. Similarly, mha007 splits into smaller strands before attaching to the little finger's bones.
Note: *Although muscle mla006 is shown in this figure, it is not simulated in our simulation.*

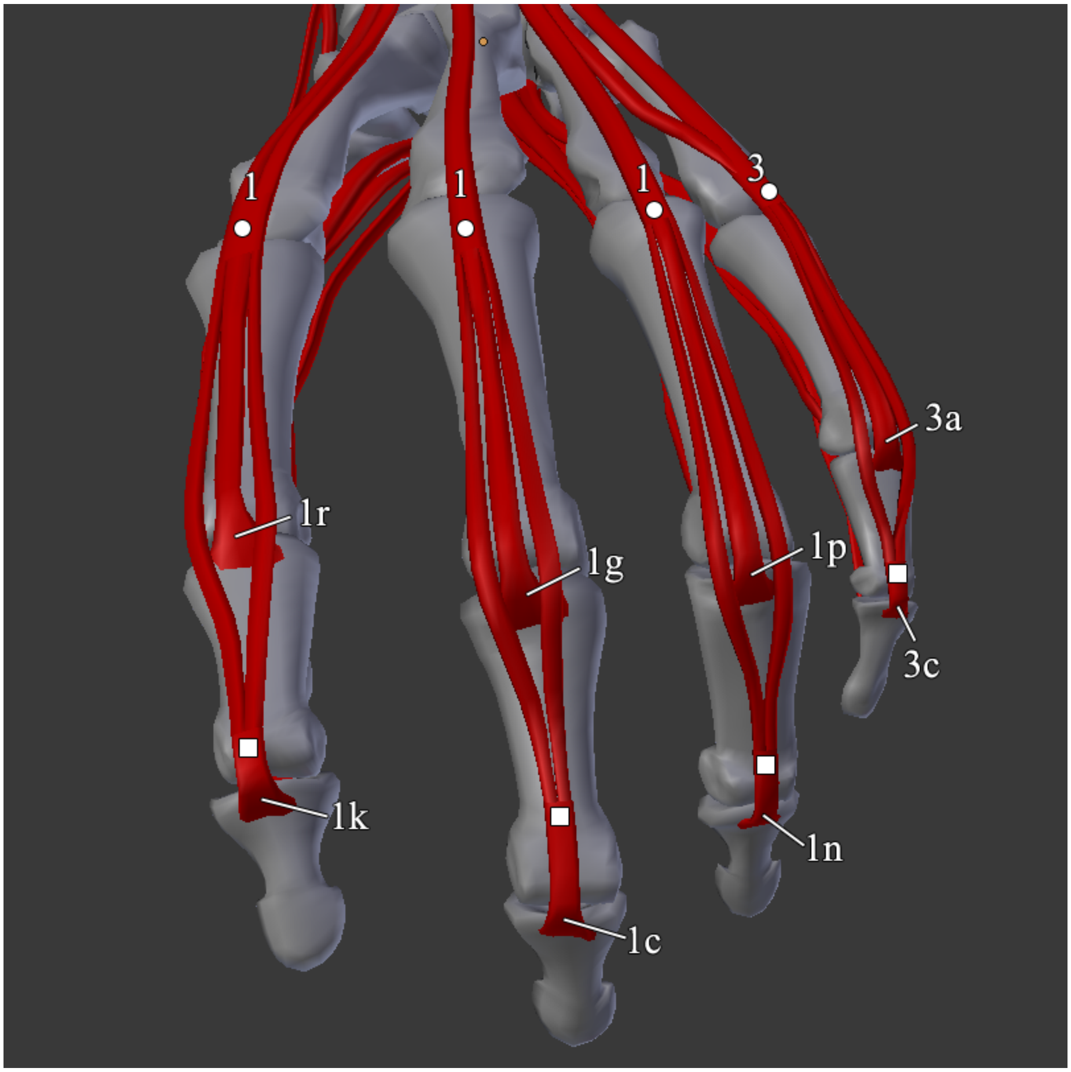

Figure A.7: **Finger upper muscles**
(1) mla005, **(3)** mha007, **(•)** Muscle splits into smaller strands, **(□)** Muscles combine into one strand

Muscles mha007 and mla005 splits into smaller strands at •, in which the smaller muscle strands attach to the intermediate phalanx and distal phalanx. For each finger, two smaller strands combine at □ to form a single muscle before attaching to the distal phalanx.
Note: *Muscle strands 1c, 1k, 1n, and 3c are simulated as individual muscle strands. No combining of muscles were simulated.*

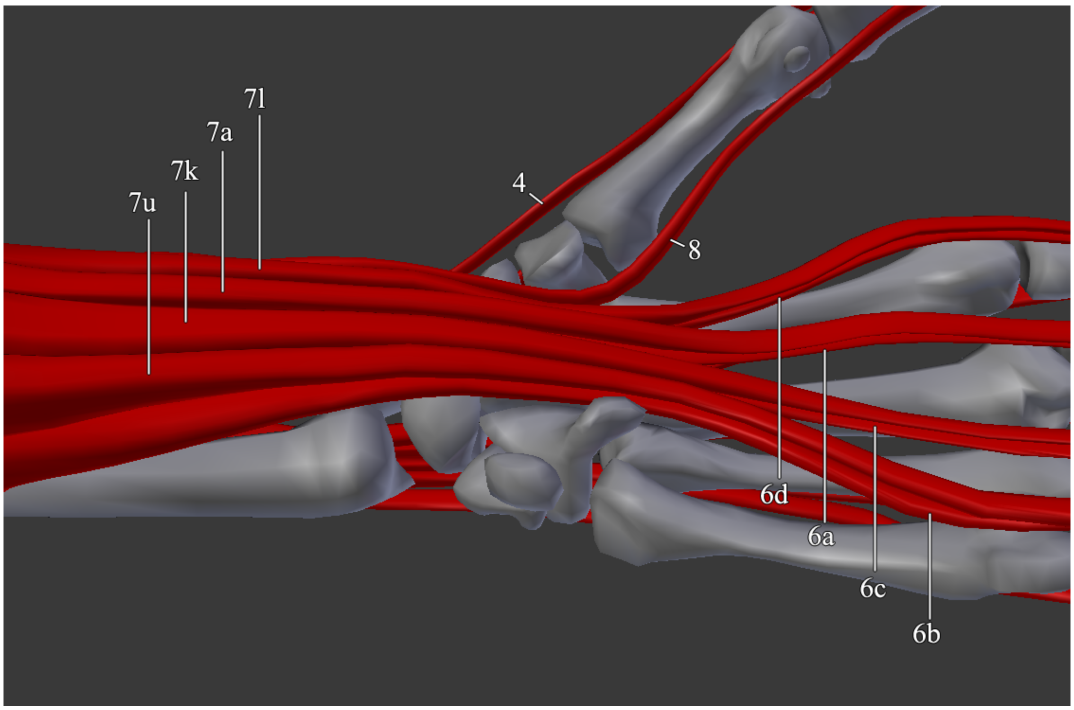

Figure A.8: **Hand lower muscles**
(4) mla007, **(6)** mla011, **(7)** mla012, **(8)** mla013

Every mla012 muscle strand is layered on top of a corresponding mla011 muscle strand.

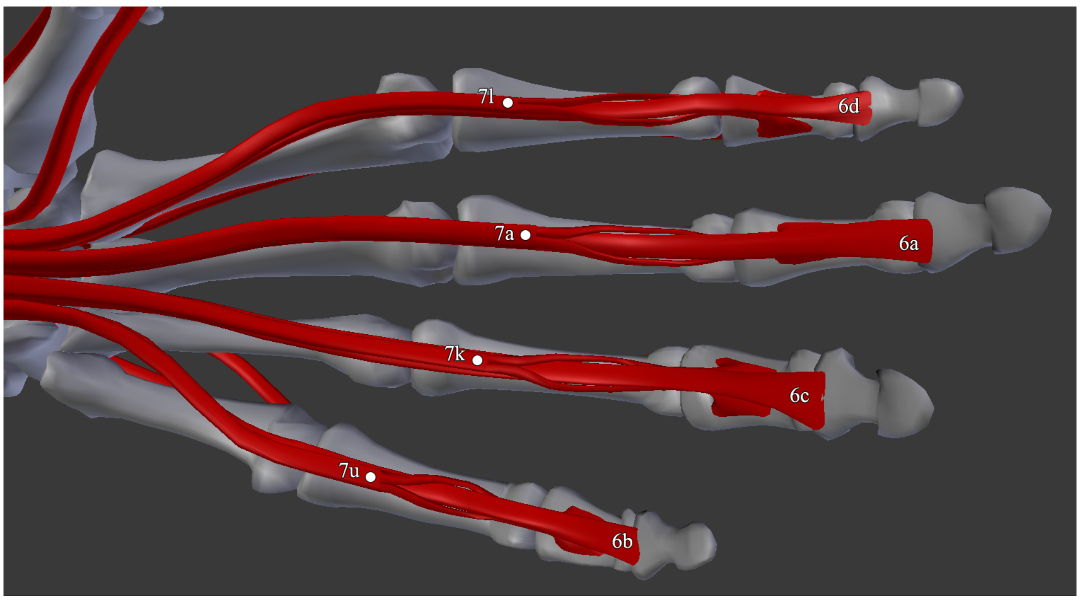

Figure A.9: **Finger lower muscles**
(6) mla011, **(7)** mla012, **(•)** Muscle splits into smaller strands

Each mla011 muscle strand runs along the hand under a mla012 muscle strand. Muscle mla012 splits at • into two smaller muscle strands that attaches at the intermediate phalanx.

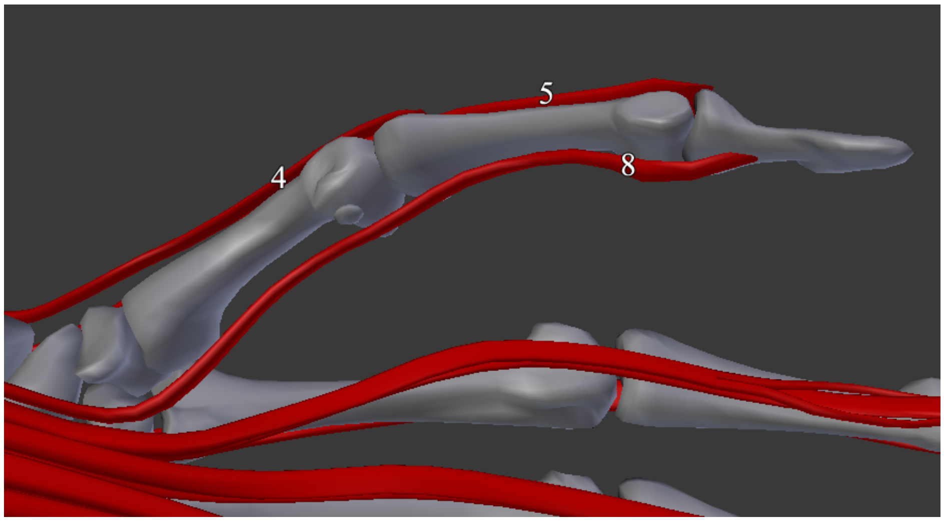

(a) Inside View of the Thumb

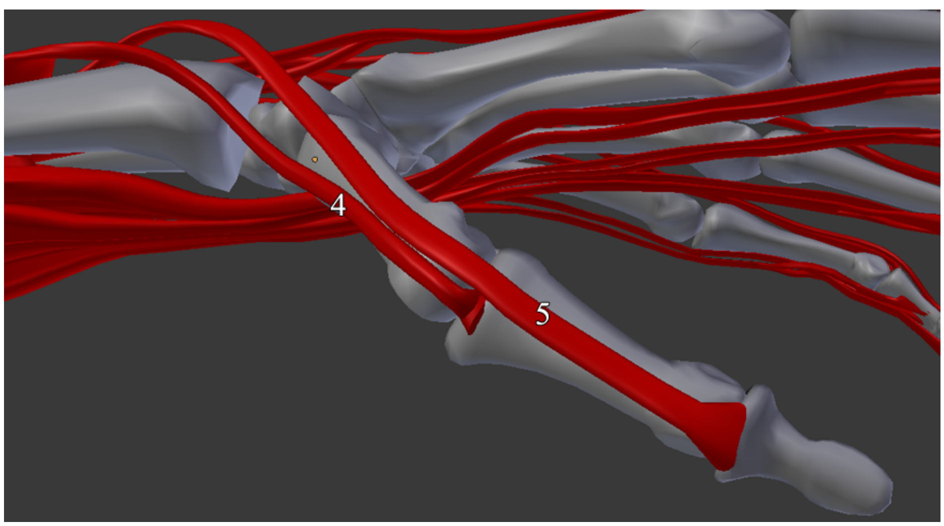

(b) Outside View of the Thumb

Figure A.10: **Thumb muscles (4)** mla007, **(5)** mla008, **(8)** mla0013

A.3.3 Wrist Muscles

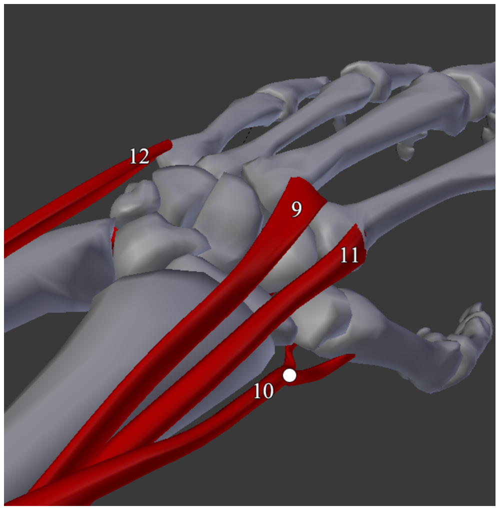

(a) Thumb-Side Angled View

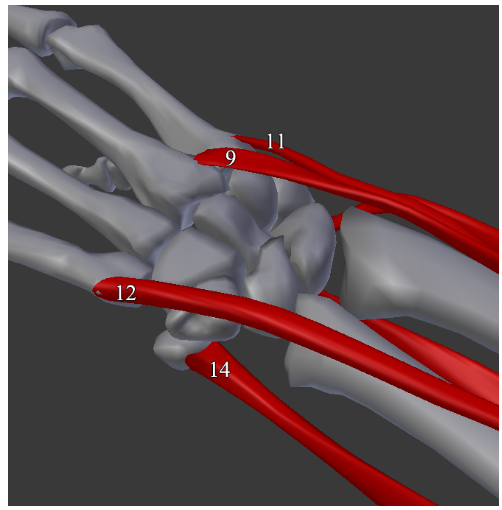

(b) Little Finger-Side Angled View

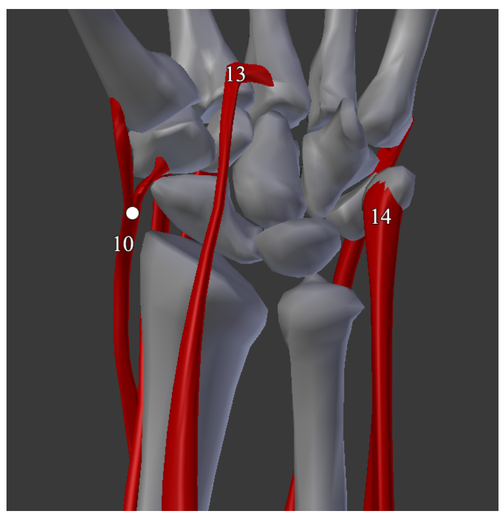

(c) Bottom View

Figure A.11: **Wrist muscles**
(9) mla002, **(10)** mha003, **(11)** mla003, **(12)** mla004, **(13)** mla008, **(14)** mla010, (●) muscle splits into multiple strands
Note: *mha003 is a single muscle that splits into two muscle strands that attach to the wrist. This muscle is simulated as a single muscle spline, by averaging the two muscle strands.*

APPENDIX B

Bone Hierarchy

Table B.1: Bone hierarchy

Bones	**Rigid Body Name**	**Body Part**	**World Coordinates – Bone Pivot**		
			x	**y**	**z**
lsul003	lsul003_004	Forearm : Radius	473.064	-1554.420	114.962
lsul004	lsul003_004	Forearm : Ulna	473.064	-1554.420	114.962
lsul005	lsul005_012	Palm : Carpal	473.064	-1554.420	114.962
lsul006	lsul005_012	Palm : Carpal	473.064	-1554.420	114.962
lsul007	lsul005_012	Palm : Carpal	473.064	-1554.420	114.962
lsul008	lsul005_012	Palm : Carpal	473.064	-1554.420	114.962
lsul009	lsul005_012	Palm : Carpal	473.064	-1554.420	114.962
lsul010	lsul005_012	Palm : Carpal	473.064	-1554.420	114.962
lsul011	lsul005_012	Palm : Carpal	473.064	-1554.420	114.962
lsul012	lsul005_012	Palm : Carpal	473.064	-1554.420	114.962
lsul013	lsul013_033	Palm : Thumb : Metacarpal	473.064	-1554.420	114.962
lsul014	lsul014	Palm : Index : Metacarpal	473.064	-1554.420	114.962
lsul015	lsul015	Palm : Middle : Metacarpal	473.064	-1554.420	114.962
lsul016	lsul016	Palm : Ring : Metacarpal	473.064	-1554.420	114.962
lsul017	lsul017	Palm : Little : Metacarpal	473.064	-1554.420	114.962
lsul018	lsul018	Thumb : Proximal Phalanx	822.307	-1613.680	74.732
lsul019	lsul019	Index : Proximal Phalanx	868.552	-1603.970	113.032
lsul020	lsul020	Middle : Proximal Phalanx	870.099	-1577.880	118.053
lsul021	lsul021	Ring : Proximal Phalanx	863.620	-1552.250	114.337
lsul022	lsul022	Little : Proximal Phalanx	844.979	-1534.220	106.265
lsul023	lsul023	Index : Intermediate Phalanx	926.185	-1603.130	103.507
lsul024	lsul024	Middle : Intermediate Phalanx	928.807	-1574.070	101.506
lsul025	lsul025	Ring : Intermediate Phalanx	919.486	-1548.710	95.284
lsul026	lsul026	Little : Intermediate Phalanx	892.142	-1525.010	91.329
lsul027	lsul027	Thumb : Distal Phalanx	861.965	-1613.900	53.482
lsul028	lsul028	Index : Distal Phalanx	952.223	-1599.800	95.181
lsul029	lsul029	Middle : Distal Phalanx	951.855	-1572.380	77.738
lsul030	lsul030	Ring : Distal Phalanx	933.536	-1545.980	69.469
lsul031	lsul031	Little : Distal Phalanx	907.703	-1524.470	77.336
lsul033	lsul013_033	Palm : Thumb : Sesamoid	473.064	-1554.420	114.962

APPENDIX C

Muscle Control Points

Table C.1: Thumb muscle control points

Muscle Name	World Coordinate x	y	z	Parent Bone
mla007	866.56	-1617.04	49.32	lsul027
	864.58	-1618.53	50.52	lsul027
	859.83	-1619.98	52.84	lsul018
	846.96	-1622.02	61.19	lsul018
	833.76	-1623.29	70.86	lsul018
	825.59	-1622.45	76.74	lsul013
	807.86	-1614.36	91.77	lsul013
	792.14	-1606.73	107.35	lsul013
	775.65	-1601.57	122.80	lsul013
	762.48	-1597.13	130.63	lsul013
	750.74	-1593.47	134.27	lsul003_004
	740.96	-1590.51	134.62	lsul003_004
	726.32	-1584.81	131.91	lsul003_004
	714.24	-1581.07	129.09	lsul003_004
	694.88	-1575.40	126.69	lsul003_004
	675.85	-1570.98	126.62	lsul003_004
	657.04	-1567.82	126.76	lsul003_004
	638.29	-1566.03	126.52	lsul003_004
	620.94	-1564.57	125.34	lsul003_004
	605.73	-1564.02	124.18	lsul003_004
	596.71	-1563.90	123.15	lsul003_004
mla008	832.42	-1620.96	66.79	lsul018
	829.10	-1623.37	68.46	lsul018
	824.02	-1623.15	72.57	lsul013
	816.41	-1619.96	78.37	lsul013
	804.63	-1613.21	86.94	lsul013
	787.32	-1605.18	98.29	lsul013
	773.39	-1601.06	109.65	lsul013
	755.42	-1601.68	121.90	lsul013
	741.12	-1601.85	125.80	lsul003_004
	727.36	-1597.38	129.12	lsul003_004
	712.86	-1589.50	131.48	lsul003_004
	699.76	-1584.37	130.16	lsul003_004
	685.33	-1582.07	128.29	lsul003_004
	667.14	-1582.92	125.32	lsul003_004
	650.02	-1585.93	122.45	lsul003_004

Muscle Name	World Coordinate x	y	z	Parent Bone
mla013	871.34	-1607.06	47.86	lsul027
	865.46	-1605.87	50.49	lsul027
	853.73	-1610.08	56.62	lsul018
	845.89	-1612.08	61.33	lsul018
	837.82	-1610.45	65.88	lsul018
	832.84	-1607.74	69.13	lsul018
	816.67	-1600.13	82.21	lsul013
	808.41	-1592.39	88.73	lsul013
	798.70	-1581.59	97.17	lsul013
	789.05	-1578.24	100.93	lsul013
	774.57	-1578.43	100.07	lsul013
	760.19	-1580.49	98.84	lsul013
	743.31	-1582.92	101.39	lsul003_004
	728.57	-1584.93	104.16	lsul003_004
	711.84	-1586.84	105.25	lsul003_004
	691.35	-1586.57	106.30	lsul003_004
	670.04	-1584.94	106.90	lsul003_004
	642.17	-1581.92	107.74	lsul003_004
	613.75	-1578.18	108.34	lsul003_004
	587.86	-1575.01	109.09	lsul003_004
	564.67	-1572.59	109.41	lsul003_004
	548.37	-1571.23	110.36	lsul003_004
	537.20	-1570.81	111.95	lsul003_004

Table C.2: Index finger muscle control points

Muscle Name	World Coordinate			Parent Bone
	x	y	z	
mla005k	957.03	-1599.70	92.55	lsul028
	956.33	-1600.57	95.47	lsul028
	953.49	-1601.47	98.81	lsul023
	948.82	-1601.93	101.81	lsul023
	940.45	-1603.52	105.05	lsul023
	928.93	-1605.04	110.86	lsul019
	915.22	-1606.26	113.46	lsul019
	900.77	-1606.95	115.89	lsul019
	889.00	-1606.61	118.62	lsul019
	876.27	-1605.48	120.58	lsul019
	864.67	-1603.71	121.78	lsul014
	845.79	-1599.27	123.29	lsul014
	830.90	-1594.72	124.35	lsul014
	806.36	-1588.55	129.00	lsul014
	789.94	-1584.18	133.23	lsul014
	769.16	-1579.19	134.03	lsul003_004
	752.69	-1575.38	135.27	lsul003_004
	737.08	-1572.94	135.25	lsul003_004
	725.66	-1572.87	134.31	lsul003_004
	711.50	-1574.68	133.01	lsul003_004
	696.32	-1578.52	133.21	lsul003_004
	682.80	-1582.22	134.03	lsul003_004
	665.03	-1587.11	134.64	lsul003_004
	645.91	-1591.76	133.85	lsul003_004
	625.43	-1595.18	132.56	lsul003_004
	604.55	-1597.27	130.83	lsul003_004
	581.34	-1599.17	127.89	lsul003_004
	558.35	-1600.15	125.39	lsul003_004
	536.22	-1599.96	123.16	lsul003_004
	517.01	-1598.78	121.98	lsul003_004
	497.36	-1596.23	120.65	lsul003_004
	481.95	-1593.48	119.26	lsul003_004
	468.13	-1590.99	117.95	lsul003_004
	459.15	-1588.91	117.54	lsul003_004
mla005r	935.11	-1602.70	104.37	lsul023
	931.94	-1603.26	106.65	lsul023
	928.06	-1604.35	109.04	lsul019
	914.24	-1605.43	111.23	lsul019
	900.19	-1606.24	114.56	lsul019
	888.45	-1605.95	117.35	lsul019
	876.27	-1605.48	120.58	lsul019
	864.67	-1603.71	121.78	lsul014
	845.79	-1599.27	123.29	lsul014
	830.90	-1594.72	124.35	lsul014
	806.36	-1588.55	129.00	lsul014
	789.94	-1584.18	133.23	lsul014
	769.16	-1579.19	134.03	lsul003_004
	752.69	-1575.38	135.27	lsul003_004
	737.08	-1572.94	135.25	lsul003_004
	725.66	-1572.87	134.31	lsul003_004
	711.50	-1574.68	133.01	lsul003_004
	696.32	-1578.52	133.21	lsul003_004
	682.80	-1582.22	134.03	lsul003_004
	665.03	-1587.11	134.64	lsul003_004
	645.91	-1591.76	133.85	lsul003_004
	625.43	-1595.18	132.56	lsul003_004
	604.55	-1597.27	130.83	lsul003_004
	581.34	-1599.17	127.89	lsul003_004
	558.35	-1600.15	125.39	lsul003_004
	536.22	-1599.96	123.16	lsul003_004
	517.01	-1598.78	121.98	lsul003_004
	497.36	-1596.23	120.65	lsul003_004
	481.95	-1593.48	119.26	lsul003_004
	468.13	-1590.99	117.95	lsul003_004
	459.15	-1588.91	117.54	lsul003_004

Muscle Name	World Coordinate			Parent Bone
	x	y	z	
mla011d	953.43	-1598.59	89.20	lsul028
	950.94	-1598.89	90.71	lsul028
	945.04	-1600.09	93.53	lsul023
	938.36	-1600.43	94.06	lsul023
	930.42	-1601.26	94.53	lsul023
	914.60	-1602.40	100.59	lsul019
	903.17	-1603.30	104.14	lsul019
	889.00	-1603.67	103.93	lsul019
	877.02	-1603.64	103.06	lsul019
	854.05	-1601.86	103.47	lsul014
	845.16	-1598.74	104.43	lsul014
	831.50	-1593.70	107.44	lsul014
	822.25	-1587.73	108.34	lsul014
	808.21	-1579.33	106.18	lsul014
	792.68	-1573.68	104.00	lsul014
	776.71	-1574.36	101.98	lsul014
	762.72	-1574.67	100.02	lsul003_004
	749.61	-1575.40	100.42	lsul003_004
	733.63	-1575.46	103.26	lsul003_004
	714.39	-1575.65	107.00	lsul003_004
	693.99	-1574.39	107.77	lsul003_004
	672.90	-1572.84	106.73	lsul003_004
	648.86	-1571.14	106.45	lsul003_004
	624.95	-1569.04	107.25	lsul003_004
	606.77	-1567.40	108.68	lsul003_004
	588.56	-1565.88	110.85	lsul003_004
	571.28	-1564.49	114.38	lsul003_004
	559.59	-1563.45	119.71	lsul003_004
	550.76	-1562.58	125.18	lsul003_004
mla012l	945.97	-1600.26	96.09	lsul023
	938.28	-1600.79	96.42	lsul023
	930.11	-1601.62	96.88	lsul023
	916.82	-1602.32	101.20	lsul019
	907.77	-1602.58	102.54	lsul019
	896.12	-1603.52	102.42	lsul019
	886.21	-1603.47	102.48	lsul019
	881.21	-1603.76	101.63	lsul019
	846.52	-1599.06	101.16	lsul014
	841.01	-1597.33	102.32	lsul014
	820.47	-1586.46	105.06	lsul014
	804.99	-1577.03	102.34	lsul014
	794.60	-1573.75	100.37	lsul014
	779.39	-1574.17	99.65	lsul014
	761.02	-1572.92	96.56	lsul014
	742.59	-1577.04	96.83	lsul003_004
	724.53	-1577.82	97.81	lsul003_004
	709.69	-1578.74	99.03	lsul003_004
	693.77	-1580.21	99.46	lsul003_004
	678.48	-1581.40	99.34	lsul003_004
	661.80	-1581.90	99.30	lsul003_004
	647.27	-1582.34	100.25	lsul003_004
	635.86	-1582.99	102.20	lsul003_004
	627.72	-1585.60	104.75	lsul003_004
	622.17	-1589.30	108.88	lsul003_004

Table C.3: Middle finger muscle control points

Muscle	World Coordinate			Parent
Name	x	y	z	Bone
mla005c	957.00	-1572.20	73.00	lsul029
	958.01	-1572.53	76.44	lsul029
	957.77	-1572.57	78.88	lsul024
	955.69	-1572.34	81.28	lsul024
	950.56	-1572.76	85.60	lsul024
	943.26	-1573.75	92.79	lsul024
	939.23	-1576.17	103.95	lsul024
	935.24	-1577.07	108.65	lsul020
	924.68	-1577.35	112.01	lsul020
	897.27	-1578.23	121.06	lsul020
	883.60	-1578.77	125.23	lsul020
	876.65	-1578.60	126.73	lsul015
	869.63	-1578.49	127.62	lsul015
	827.11	-1575.26	127.45	lsul015
	799.23	-1574.78	131.45	lsul015
	777.92	-1573.83	133.51	lsul003_004
	763.86	-1572.91	135.23	lsul003_004
	749.00	-1571.44	135.37	lsul003_004
	737.06	-1570.97	134.54	lsul003_004
	725.67	-1570.96	133.66	lsul003_004
	713.54	-1572.13	133.00	lsul003_004
	700.73	-1574.02	132.76	lsul003_004
	686.46	-1577.63	133.84	lsul003_004
	671.41	-1582.31	135.01	lsul003_004
	654.17	-1586.62	134.93	lsul003_004
	633.35	-1589.78	134.64	lsul003_004
	613.11	-1591.93	134.12	lsul003_004
	589.19	-1594.31	132.21	lsul003_004
	565.56	-1595.53	129.72	lsul003_004
	545.91	-1595.83	127.40	lsul003_004
	526.94	-1596.03	125.17	lsul003_004
	509.94	-1595.22	123.44	lsul003_004
	494.80	-1594.11	121.81	lsul003_004
	481.03	-1592.14	119.86	lsul003_004
mla005g	938.54	-1573.92	98.32	lsul024
	937.04	-1576.00	104.28	lsul024
	932.91	-1576.60	107.14	lsul020
	927.98	-1576.75	109.05	lsul020
	917.60	-1576.37	110.37	lsul020
	908.39	-1576.85	114.62	lsul020
	897.27	-1578.23	121.06	lsul020
	883.60	-1578.77	125.23	lsul020
	876.65	-1578.60	126.73	lsul015
	869.63	-1578.49	127.62	lsul015
	827.11	-1575.26	127.45	lsul015
	799.23	-1574.78	131.45	lsul015
	777.92	-1573.83	133.51	lsul003_004
	763.86	-1572.91	135.23	lsul003_004
	749.00	-1571.44	135.37	lsul003_004
	737.06	-1570.97	134.54	lsul003_004
	725.67	-1570.96	133.66	lsul003_004
	713.54	-1572.13	133.00	lsul003_004
	700.73	-1574.02	132.76	lsul003_004
	686.46	-1577.63	133.84	lsul003_004
	671.41	-1582.31	135.01	lsul003_004
	654.17	-1586.62	134.93	lsul003_004
	633.35	-1589.78	134.64	lsul003_004
	613.11	-1591.93	134.12	lsul003_004
	589.19	-1594.31	132.21	lsul003_004
	565.56	-1595.53	129.72	lsul003_004
	545.91	-1595.83	127.40	lsul003_004
	526.94	-1596.03	125.17	lsul003_004
	509.94	-1595.22	123.44	lsul003_004
	494.80	-1594.11	121.81	lsul003_004
	481.03	-1592.14	119.86	lsul003_004

Muscle	World Coordinate			Parent
Name	x	y	z	Bone
mla011a	951.81	-1570.39	70.57	lsul029
	946.46	-1571.55	75.19	lsul024
	935.09	-1572.41	85.51	lsul024
	929.55	-1572.68	89.81	lsul024
	923.75	-1573.47	94.25	lsul020
	911.59	-1575.21	103.57	lsul020
	904.54	-1575.97	105.76	lsul020
	889.86	-1577.26	107.14	lsul020
	880.69	-1577.74	106.70	lsul020
	868.27	-1577.88	104.91	lsul015
	846.01	-1577.50	104.69	lsul003_004
	829.62	-1574.69	104.96	lsul003_004
	814.62	-1571.58	105.48	lsul003_004
	803.79	-1569.73	104.82	lsul003_004
	784.37	-1569.40	102.21	lsul003_004
	767.13	-1569.76	100.40	lsul003_004
	755.42	-1570.32	100.94	lsul003_004
	744.07	-1569.89	102.61	lsul003_004
	727.72	-1568.49	105.90	lsul003_004
	710.70	-1567.32	108.95	lsul003_004
	692.58	-1566.37	110.20	lsul003_004
	675.61	-1564.55	109.34	lsul003_004
	655.63	-1562.23	108.84	lsul003_004
	632.64	-1559.26	109.25	lsul003_004
	610.34	-1556.73	109.92	lsul003_004
	588.22	-1555.16	111.83	lsul003_004
	566.41	-1554.03	115.33	lsul003_004
	546.05	-1553.76	119.25	lsul003_004
	532.28	-1554.40	123.87	lsul003_004
	522.08	-1556.34	130.12	lsul003_004
mla012a	945.66	-1572.76	82.47	lsul024
	932.70	-1572.83	90.21	lsul024
	928.82	-1572.95	92.41	lsul024
	923.81	-1573.29	97.31	lsul020
	914.29	-1574.37	103.56	lsul020
	904.40	-1576.05	105.80	lsul020
	893.18	-1577.03	104.59	lsul020
	876.54	-1577.73	103.67	lsul020
	865.81	-1577.95	103.54	lsul015
	854.40	-1577.66	104.21	lsul015
	835.28	-1575.99	102.42	lsul015
	814.94	-1571.53	103.44	lsul003_004
	797.65	-1569.61	100.60	lsul003_004
	779.21	-1570.24	98.10	lsul003_004
	761.91	-1571.33	96.94	lsul003_004
	745.56	-1571.90	97.36	lsul003_004
	723.33	-1571.75	97.70	lsul003_004
	703.95	-1571.80	98.89	lsul003_004
	682.84	-1572.38	98.48	lsul003_004
	661.20	-1571.99	97.20	lsul003_004
	641.66	-1571.31	96.59	lsul003_004
	622.47	-1570.88	96.64	lsul003_004
	603.11	-1571.77	98.60	lsul003_004
	585.93	-1573.33	101.51	lsul003_004
	572.26	-1575.49	105.18	lsul003_004
	562.86	-1578.02	108.13	lsul003_004

Table C.4: Ring finger muscle control points

Muscle Name	World Coordinate x	y	z	Parent Bone
mla005n	936.35	-1547.20	64.42	lsul030
	938.14	-1546.92	67.92	lsul030
	937.28	-1546.90	70.64	lsul025
	934.92	-1546.90	77.75	lsul025
	932.70	-1548.18	87.04	lsul025
	929.55	-1548.91	95.89	lsul025
	925.52	-1549.85	100.31	lsul021
	919.27	-1549.88	103.34	lsul021
	909.45	-1550.45	106.22	lsul021
	896.72	-1551.38	110.77	lsul021
	882.15	-1553.22	118.34	lsul021
	875.03	-1553.82	120.31	lsul021
	868.29	-1555.09	121.57	lsul016
	831.08	-1558.55	124.59	lsul016
	796.32	-1565.01	130.53	lsul016
	776.24	-1567.41	132.13	lsul016
	762.16	-1568.38	134.99	lsul016
	748.92	-1568.32	134.90	lsul003_004
	736.99	-1567.97	134.35	lsul003_004
	725.92	-1568.12	133.64	lsul003_004
	713.41	-1569.26	133.09	lsul003_004
	700.70	-1571.00	132.79	lsul003_004
	687.00	-1574.48	133.97	lsul003_004
	671.32	-1578.63	135.22	lsul003_004
	653.32	-1582.57	135.99	lsul003_004
	633.89	-1586.46	135.59	lsul003_004
	614.50	-1589.30	134.30	lsul003_004
	594.50	-1590.20	132.21	lsul003_004
	573.17	-1590.85	129.72	lsul003_004
	549.44	-1591.70	126.72	lsul003_004
	527.91	-1592.01	124.13	lsul003_004
	508.90	-1591.94	121.82	lsul003_004
	496.04	-1591.05	120.73	lsul003_004
	482.34	-1589.00	118.80	lsul003_004
	474.07	-1587.26	116.71	lsul003_004
mla005p	927.96	-1548.92	91.15	lsul025
	927.40	-1549.44	95.25	lsul025
	924.80	-1549.91	98.25	lsul021
	914.95	-1550.03	103.23	lsul021
	902.70	-1550.31	107.00	lsul021
	890.99	-1551.65	113.12	lsul021
	882.15	-1553.22	118.34	lsul021
	875.03	-1553.82	120.31	lsul021
	868.29	-1555.09	121.57	lsul016
	831.08	-1558.55	124.59	lsul016
	796.32	-1565.01	130.53	lsul016
	776.24	-1567.41	132.13	lsul016
	762.16	-1568.38	134.99	lsul016
	748.92	-1568.32	134.90	lsul003_004
	736.99	-1567.97	134.35	lsul003_004
	725.92	-1568.12	133.64	lsul003_004
	713.41	-1569.26	133.09	lsul003_004
	700.70	-1571.00	132.79	lsul003_004
	687.00	-1574.48	133.97	lsul003_004
	671.32	-1578.63	135.22	lsul003_004
	653.32	-1582.57	135.99	lsul003_004
	633.89	-1586.46	135.59	lsul003_004
	614.50	-1589.30	134.30	lsul003_004
	594.50	-1590.20	132.21	lsul003_004
	573.17	-1590.85	129.72	lsul003_004
	549.44	-1591.70	126.72	lsul003_004
	527.91	-1592.01	124.13	lsul003_004
	508.90	-1591.94	121.82	lsul003_004
	496.04	-1591.05	120.73	lsul003_004
	482.34	-1589.00	118.80	lsul003_004
	474.07	-1587.26	116.71	lsul003_004

Muscle Name	World Coordinate x	y	z	Parent Bone
mla011c	931.55	-1546.76	63.19	lsul030
	930.74	-1546.71	65.20	lsul030
	928.75	-1547.35	68.73	lsul025
	925.05	-1547.87	76.64	lsul025
	917.94	-1548.99	86.30	lsul025
	908.91	-1549.51	94.08	lsul021
	900.26	-1549.96	97.17	lsul021
	884.33	-1551.24	102.32	lsul021
	869.48	-1553.10	104.88	lsul021
	856.60	-1554.89	106.65	lsul016
	823.83	-1561.26	108.34	lsul016
	801.41	-1564.03	106.12	lsul016
	778.64	-1564.82	103.83	lsul016
	764.02	-1564.37	101.75	lsul016
	751.99	-1563.82	103.06	lsul003_004
	738.65	-1563.01	105.41	lsul003_004
	725.33	-1561.38	108.31	lsul003_004
	710.72	-1560.04	110.37	lsul003_004
	696.74	-1558.46	111.72	lsul003_004
	683.31	-1556.46	111.95	lsul003_004
	668.23	-1553.63	111.18	lsul003_004
	650.40	-1549.83	111.01	lsul003_004
	635.47	-1546.46	112.04	lsul003_004
	619.99	-1543.71	113.35	lsul003_004
	602.91	-1543.13	118.35	lsul003_004
	590.02	-1546.07	123.45	lsul003_004
	578.54	-1550.19	127.73	lsul003_004
	572.17	-1557.70	131.90	lsul003_004
mla012k	928.26	-1547.48	74.34	lsul025
	923.07	-1548.90	82.87	lsul025
	918.51	-1549.09	88.49	lsul025
	912.84	-1549.01	93.05	lsul021
	907.57	-1549.42	95.36	lsul021
	893.53	-1550.58	98.01	lsul021
	884.08	-1551.57	99.86	lsul021
	871.22	-1553.21	102.47	lsul016
	852.27	-1555.99	105.10	lsul016
	833.22	-1559.01	106.33	lsul016
	816.98	-1562.47	105.70	lsul016
	796.35	-1565.36	101.94	lsul016
	777.27	-1564.60	99.60	lsul016
	760.00	-1564.78	98.56	lsul016
	742.54	-1564.75	98.90	lsul003_004
	720.89	-1563.84	99.99	lsul003_004
	700.57	-1562.69	100.05	lsul003_004
	677.46	-1560.64	97.60	lsul003_004
	654.76	-1558.96	95.26	lsul003_004
	629.54	-1555.78	93.57	lsul003_004
	607.29	-1552.69	93.91	lsul003_004
	585.76	-1549.41	96.22	lsul003_004
	562.06	-1545.46	100.47	lsul003_004
	537.63	-1542.41	107.05	lsul003_004
	525.31	-1541.91	110.46	lsul003_004
	512.81	-1541.67	114.50	lsul003_004
	501.51	-1543.64	118.38	lsul003_004
	491.77	-1545.83	122.45	lsul003_004

Table C.5: Little finger muscle control points

Muscle	World Coordinate			Parent
Name	**x**	**y**	**z**	**Bone**
mha007c	912.20	-1524.39	75.52	lsul031
	912.40	-1524.25	77.46	lsul031
	909.11	-1524.00	82.57	lsul026
	904.42	-1523.64	88.61	lsul026
	900.37	-1523.56	93.92	lsul026
	896.43	-1524.14	97.75	lsul022
	889.40	-1525.26	100.96	lsul022
	873.15	-1528.06	106.77	lsul022
	865.53	-1529.79	109.74	lsul022
	859.16	-1531.15	111.34	lsul022
	853.41	-1532.64	112.92	lsul017
	840.12	-1536.74	116.05	lsul017
	810.94	-1546.05	121.02	lsul017
	799.07	-1549.84	123.76	lsul017
	781.03	-1555.40	127.80	lsul017
	768.35	-1557.53	130.98	lsul017
	755.97	-1558.46	132.59	lsul017
	740.43	-1559.58	132.97	lsul003_004
	725.88	-1561.73	133.12	lsul003_004
	713.16	-1563.75	133.54	lsul003_004
	695.04	-1567.37	134.87	lsul003_004
	666.69	-1573.39	136.70	lsul003_004
	631.34	-1579.77	136.92	lsul003_004
	594.43	-1585.87	135.45	lsul003_004
	556.40	-1588.56	133.05	lsul003_004
	529.32	-1591.42	129.13	lsul003_004
	503.75	-1591.10	126.01	lsul003_004
	485.54	-1589.89	124.29	lsul003_004
	478.23	-1589.02	122.03	lsul003_004
	469.74	-1586.47	119.79	lsul003_004
mha007a	899.49	-1523.90	90.73	lsul026
	899.18	-1524.31	92.88	lsul026
	896.44	-1524.28	95.65	lsul022
	891.29	-1524.69	98.05	lsul022
	872.07	-1527.80	104.80	lsul022
	863.07	-1530.07	109.48	lsul022
	859.10	-1531.12	110.51	lsul022
	853.41	-1532.64	112.92	lsul017
	840.12	-1536.74	116.05	lsul017
	810.94	-1546.05	121.02	lsul017
	799.07	-1549.84	123.76	lsul017
	781.03	-1555.40	127.80	lsul017
	768.35	-1557.53	130.98	lsul017
	755.97	-1558.46	132.59	lsul017
	740.43	-1559.58	132.97	lsul003_004
	725.88	-1561.73	133.12	lsul003_004
	713.16	-1563.75	133.54	lsul003_004
	695.04	-1567.37	134.87	lsul003_004
	666.69	-1573.39	136.70	lsul003_004
	631.34	-1579.77	136.92	lsul003_004
	594.43	-1585.87	135.45	lsul003_004
	556.40	-1588.56	133.05	lsul003_004
	529.32	-1591.42	129.13	lsul003_004
	503.75	-1591.10	126.01	lsul003_004
	485.54	-1589.89	124.29	lsul003_004
	478.23	-1589.02	122.03	lsul003_004
	469.74	-1586.47	119.79	lsul003_004

Muscle	World Coordinate			Parent
Name	**x**	**y**	**z**	**Bone**
mla011b	909.01	-1524.97	72.16	lsul031
	907.21	-1524.69	73.82	lsul031
	903.67	-1524.74	77.28	lsul026
	898.87	-1525.57	82.13	lsul026
	895.47	-1526.29	84.37	lsul026
	886.37	-1527.35	88.75	lsul022
	877.40	-1528.54	93.97	lsul022
	865.32	-1530.50	96.85	lsul022
	853.71	-1533.30	97.57	lsul022
	836.04	-1538.76	104.54	lsul017
	826.53	-1544.51	105.19	lsul017
	815.29	-1553.54	107.05	lsul017
	802.88	-1558.93	107.79	lsul017
	789.49	-1560.24	107.03	lsul017
	769.33	-1560.85	104.14	lsul017
	758.26	-1558.83	104.27	lsul017
	747.72	-1557.61	104.83	lsul003_004
	730.75	-1555.00	108.18	lsul003_004
	714.36	-1552.48	111.87	lsul003_004
	689.14	-1546.63	113.85	lsul003_004
	667.16	-1540.67	115.77	lsul003_004
	649.14	-1537.22	120.43	lsul003_004
	631.13	-1539.98	127.88	lsul003_004
	618.26	-1545.68	132.27	lsul003_004
	609.61	-1551.20	133.81	lsul003_004
	606.82	-1559.33	133.18	lsul003_004
mla012u	903.81	-1524.64	80.16	lsul026
	895.46	-1525.59	85.80	lsul026
	889.09	-1526.70	88.24	lsul022
	879.38	-1528.36	91.10	lsul022
	853.69	-1532.56	97.00	lsul022
	833.75	-1540.33	101.22	lsul017
	822.00	-1549.78	103.29	lsul017
	803.47	-1559.27	102.69	lsul017
	782.81	-1559.63	101.68	lsul017
	761.35	-1559.87	98.93	lsul017
	729.59	-1556.54	101.61	lsul003_004
	702.58	-1552.21	102.11	lsul003_004
	669.94	-1545.52	99.11	lsul003_004
	646.41	-1539.58	95.77	lsul003_004
	604.05	-1532.95	98.46	lsul003_004
	569.46	-1528.46	103.48	lsul003_004
	539.91	-1525.16	108.10	lsul003_004
	508.71	-1522.05	114.31	lsul003_004
	489.88	-1519.77	117.94	lsul003_004
	472.36	-1516.54	121.11	lsul003_004
	465.80	-1515.79	122.30	lsul003_004
	458.90	-1516.63	123.43	lsul003_004

Table C.6: Wrist muscle control points

Muscle Name	World Coordinate x	y	z	Parent Bone
mla002	802.11	-1580.26	126.43	lsul005_012
	797.42	-1581.81	127.65	lsul005_012
	788.53	-1584.10	128.37	lsul005_012
	774.53	-1587.89	129.54	lsul005_012
	763.05	-1590.20	129.84	lsul003_004
	749.39	-1591.26	130.34	lsul003_004
	735.54	-1592.05	128.86	lsul003_004
	721.17	-1593.83	126.81	lsul003_004
	705.09	-1595.72	124.51	lsul003_004
	688.65	-1597.35	122.05	lsul003_004
	670.83	-1598.57	119.45	lsul003_004
	645.44	-1599.34	115.64	lsul003_004
	630.76	-1600.18	115.24	lsul003_004
	602.57	-1600.61	114.39	lsul003_004
	580.52	-1600.45	113.04	lsul003_004
	552.24	-1599.17	108.91	lsul003_004
	526.05	-1597.22	106.91	lsul003_004
	506.52	-1595.48	107.77	lsul003_004
	493.92	-1593.59	109.29	lsul003_004
	482.98	-1591.15	110.81	lsul003_004
	470.35	-1588.72	113.39	lsul003_004
mha003	785.92	-1598.38	100.54	lsul005_012
	781.68	-1599.18	99.98	lsul005_012
	777.62	-1599.51	100.33	lsul005_012
	773.87	-1599.82	102.56	lsul005_012
	770.04	-1600.41	106.80	lsul005_012
	764.64	-1602.67	115.20	lsul003_004
	760.33	-1603.45	118.57	lsul003_004
	747.76	-1603.54	121.74	lsul003_004
	734.69	-1601.87	124.22	lsul003_004
	723.32	-1599.63	127.40	lsul003_004
	708.03	-1596.57	129.57	lsul003_004
	695.77	-1592.08	130.18	lsul003_004
	681.05	-1588.46	130.35	lsul003_004
	664.38	-1586.17	129.98	lsul003_004
	646.69	-1584.77	128.89	lsul003_004
	629.60	-1584.09	127.21	lsul003_004
	612.18	-1584.15	127.33	lsul003_004
	596.35	-1582.54	127.60	lsul003_004
	582.95	-1580.16	127.43	lsul003_004
	569.59	-1578.23	127.62	lsul003_004
	555.21	-1576.90	128.04	lsul003_004
	541.91	-1575.87	129.83	lsul003_004
	528.21	-1574.38	132.19	lsul003_004
mla003	801.47	-1594.98	120.62	lsul005_012
	797.45	-1595.71	121.64	lsul005_012
	790.83	-1596.44	122.81	lsul005_012
	776.59	-1595.97	123.78	lsul005_012
	760.61	-1596.85	125.28	lsul003_004
	746.53	-1597.40	125.36	lsul003_004
	728.14	-1596.31	123.35	lsul003_004
	709.46	-1597.67	121.07	lsul003_004
	693.62	-1598.65	119.08	lsul003_004
	679.10	-1598.68	116.09	lsul003_004
	663.13	-1599.11	113.05	lsul003_004
	647.27	-1599.83	110.05	lsul003_004
	629.56	-1601.26	107.64	lsul003_004
	613.98	-1603.02	105.93	lsul003_004
	594.75	-1605.11	104.45	lsul003_004
	558.31	-1605.99	101.42	lsul003_004
	539.18	-1605.47	100.30	lsul003_004
	519.92	-1604.65	100.07	lsul003_004
	501.94	-1603.69	101.64	lsul003_004
	486.13	-1602.70	104.05	lsul003_004
	468.60	-1600.68	107.77	lsul003_004
	454.68	-1597.30	111.30	lsul003_004
	443.28	-1592.72	113.71	lsul003_004
	435.32	-1586.09	114.88	lsul003_004
	429.74	-1576.27	115.13	lsul003_004
	647.27	-1599.83	110.05	lsul003_004
	629.56	-1601.26	107.64	lsul003_004
	613.98	-1603.02	105.93	lsul003_004
	594.75	-1605.11	104.45	lsul003_004
	558.31	-1605.99	101.42	lsul003_004
	539.18	-1605.47	100.30	lsul003_004
	519.92	-1604.65	100.07	lsul003_004
	501.94	-1603.69	101.64	lsul003_004
	486.13	-1602.70	104.05	lsul003_004
	468.60	-1600.68	107.77	lsul003_004
	454.68	-1597.30	111.30	lsul003_004
	443.28	-1592.72	113.71	lsul003_004
	435.32	-1586.09	114.88	lsul003_004
	429.74	-1576.27	115.13	lsul003_004
mla004	798.30	-1538.42	119.10	lsul005_012
	791.04	-1540.68	121.67	lsul005_012
	782.53	-1543.88	124.65	lsul005_012
	773.09	-1546.99	127.68	lsul005_012
	759.57	-1550.37	130.58	lsul003_004
	744.72	-1552.67	132.44	lsul003_004
	731.28	-1554.78	133.01	lsul003_004
	716.67	-1557.21	133.57	lsul003_004
	702.15	-1559.31	134.38	lsul003_004
	687.99	-1561.35	135.14	lsul003_004
	673.10	-1563.01	136.23	lsul003_004
	656.25	-1564.97	137.28	lsul003_004
	640.43	-1567.36	138.01	lsul003_004
	623.97	-1570.20	137.97	lsul003_004
	607.15	-1572.90	137.92	lsul003_004
	588.36	-1575.81	137.92	lsul003_004
	567.52	-1578.94	137.39	lsul003_004
	547.06	-1582.08	136.03	lsul003_004
	527.99	-1584.43	133.89	lsul003_004
	512.41	-1586.01	131.92	lsul003_004
	494.73	-1586.76	129.02	lsul003_004
	480.93	-1586.41	126.59	lsul003_004
	470.37	-1585.36	124.72	lsul003_004
	460.80	-1584.09	122.78	lsul003_004
mla008	806.57	-1577.25	112.85	lsul005_012
	804.07	-1579.44	109.43	lsul005_012
	800.94	-1580.60	107.21	lsul005_012
	790.52	-1581.36	102.91	lsul005_012
	776.89	-1581.40	99.73	lsul005_012
	759.68	-1583.75	97.45	lsul003_004
	741.41	-1585.91	96.64	lsul003_004
	718.03	-1586.85	96.81	lsul003_004
	698.54	-1585.74	96.66	lsul003_004
	677.59	-1583.19	93.20	lsul003_004
	658.09	-1580.60	88.90	lsul003_004
	638.19	-1577.60	85.83	lsul003_004
	617.05	-1573.46	84.11	lsul003_004
	595.15	-1567.81	82.74	lsul003_004
	574.71	-1560.57	82.01	lsul003_004
	552.99	-1551.23	81.84	lsul003_004
	532.46	-1541.46	84.04	lsul003_004
	515.76	-1532.90	87.86	lsul003_004
	500.89	-1525.93	93.65	lsul003_004
	488.92	-1521.31	98.86	lsul003_004
	478.18	-1518.53	105.09	lsul003_004
	470.29	-1517.51	110.79	lsul003_004
	464.61	-1517.30	115.27	lsul003_004
	458.32	-1517.76	121.01	lsul003_004
mla010	773.16	-1546.67	108.11	lsul005_012
	767.19	-1546.61	108.01	lsul005_012
	756.65	-1546.22	107.92	lsul003_004
	743.30	-1545.36	108.22	lsul003_004
	726.97	-1544.07	109.48	lsul003_004
	705.11	-1541.77	111.29	lsul003_004
	688.35	-1539.07	112.16	lsul003_004
	669.44	-1534.66	114.45	lsul003_004
	650.46	-1530.75	116.45	lsul003_004
	626.38	-1526.03	117.70	lsul003_004
	606.42	-1522.95	119.11	lsul003_004
	584.44	-1520.79	121.17	lsul003_004
	561.50	-1519.62	122.85	lsul003_004
	536.07	-1519.28	124.33	lsul003_004
	508.84	-1520.01	127.66	lsul003_004
	487.99	-1521.65	129.43	lsul003_004
	468.33	-1523.63	130.70	lsul003_004

Bibliography

Albrecht, I., Haber, J., and Seidel, H. (2003). Construction and animation of anatomically based human hand models. In *Proceedings of the 2003 ACM SIGGRAPH/Eurographics symposium on Computer animation*, pages 98–109. Eurographics Association. 7

Audenaert, A. and Audenaert, E. (2008). Global optimization method for combined spherical-cylindrical wrapping in musculoskeletal upper limb modelling. *Comput. Methods Prog. Biomed.*, 92:8–19. 7

Der, K., Sumner, R., and Popović, J. (2006). Inverse kinematics for reduced deformable models. In *ACM SIGGRAPH 2006*, pages 1174–1179. ACM. 5

Easterling, D., Watson, L., and Madigan, M. (2011). Direct search versus simulated annealing on two high dimensional problems. In *Proceedings of the 19th High Performance Computing Symposia*, pages 89–95. Society for Computer Simulation International. 6

ElKoura, G. and Singh, K. (2003). Handrix: Animating the human hand. In *Proceedings of the 2003 ACM SIGGRAPH/Eurographics Symposium on Computer Animation*, pages 110–119. Eurographics Association. 7

Faloutsos, P., van de Panne, M., and Terzopoulos, D. (2001). Composable controllers for physics-based character animation. In *Proceedings of the 28th Annual Conference on Computer Graphics and Interactive Techniques (ACM SIGGRAPH)*, pages 251–260. ACM. 6

Fêdor, M. (2003). Application of inverse kinematics for skeleton manipulation in real-time. In *Proceedings of the 19th Spring Conference on Computer Graphics*, pages 203–212. ACM. 5

Grochow, K., Martin, S., Hertzmann, A., and Popović, Z. (2004). Style-based inverse kinematics. *ACM Transactions on Graphics*, 23:522–531. 5

Ho, E., Komura, T., and Lau, R. (2005). Computing inverse kinematics with linear programming. In *Proceedings of the ACM Symposium on Virtual Reality Software and Technology*, pages 163–166. ACM. 4

Hodgkinson, G. (2009). The seduction of realism. In *ACM SIGGRAPH ASIA 2009 Educators Program*, pages 4:1–4:4. ACM. 1

Lai, J. and Chao, M. (1989). Parallel algorithm and VLSI architecture for a robot's inverse kinematics. In *Proceedings of the 1989 ACM/IEEE Conference on Supercomputing*, pages 123–132. ACM. 5

Lee, J. and Shin, S. (1999). A hierarchical approach to interactive motion editing for human-like figures. In *Proceedings of the 26th annual Conference on Computer Graphics and Interactive Techniques (ACM SIGGRAPH)*, pages 39–48. ACM Press/Addison-Wesley Publishing Co. 5

Lee, S., Sifakis, E., and Terzopoulos, D. (2009). Comprehensive biomechanical modeling and simulation of the upper body. *ACM Transactions on Graphics*, 28:99:1–99:17. 7, 30, 31

Lee, S. and Terzopoulos, D. (2006). Heads up! Biomechanical modeling and neuromuscular control of the neck. *ACM Transactions on Graphics*, 25:1188–1198. 7, 13, 14

Lee, Y., Terzopoulos, D., and Waters, K. (1995). Realistic modeling for facial animation. In *Proceedings of the 22nd Annual Conference on Computer Graphics and Interactive Techniques (ACM SIGGRAPH)*, pages 55–62. ACM. 7

McKenna, M. and Zeltzer, D. (1990). Dynamic simulation of autonomous legged locomotion. In *Proceedings of the 17th Annual Conference on Computer Graphics and Interactive Techniques (ACM SIGGRAPH)*, pages 29–38. ACM. 6

Meredith, M. and Maddock, S. (2005). Adapting motion capture data using weighted real-time inverse kinematics. *Comput. Entertain.*, 3:5–5. 5

Ng-Thow-Hing, V. (2001). *Anatomically-Based Models for Physical and Geometric Reconstruction of Humans and Other Animals*. PhD thesis, Department of Computer Science, University of Toronto. 13

Peinado, M., Meziat, D., Maupu, D., Raunhardt, D., Thalmann, D., and Boulic, R. (2007). Accurate on-line avatar control with collision anticipation. In *Proceedings of the 2007 ACM Symposium on Virtual Reality Software and Technology*, pages 89–97. ACM. 5

Pollard, N. and Zordan, V. (2005). Physically based grasping control from example. In *Proceedings of the 2005 ACM SIGGRAPH/Eurographics Symposium on Computer Animation*, pages 311–318. ACM. 6

Pratscher, M., Coleman, P., Laszlo, J., and Singh, K. (2005). Outside-in anatomy based character rigging. In *Proceedings of the 2005 ACM SIGGRAPH/Eurographics Symposium on Computer Animation*, pages 329–338. ACM. 7

Scheepers, F., Parent, R., Carlson, W., and May, S. (1997). Anatomy-based modeling of the human musculature. In *Proceedings of the 24th Annual Conference on Computer Graphics and Interactive Techniques (ACM SIGGRAPH)*, pages 163–172. ACM Press/Addison-Wesley Publishing Co. 6, 7

Sifakis, E., Neverov, I., and Fedkiw, R. (2005). Automatic determination of facial muscle activations from sparse motion capture marker data. *ACM Transactions on Graphics*, 24:417–425. 7

Simmons, M., Wilhelms, J., and Van Gelder, A. (2002). Model-based reconstruction for creature animation. In *Proceedings of the 2002 ACM SIGGRAPH/Eurographics Symposium on Computer Animation*, pages 139–146. ACM. 6

Sueda, S., Kaufman, A., and Pai, D. (2008). Musculotendon simulation for hand animation. In *ACM SIGGRAPH 2008*, pages 83:1–83:8. ACM. 7, 11, 31

Sumner, R., Zwicker, M., Gotsman, C., and Popović, J. (2005). Mesh-based inverse kinematics. *ACM Transactions on Graphics*, 24:488–495. 5

Teran, J., Blemker, S., Ng-Thow-Hing, V., and Fedkiw, R. (2003). Finite volume methods for the simulation of skeletal muscle. In *Proceedings of the 2003 ACM SIGGRAPH/Eurographics Symposium on Computer Animation*, pages 68–74. Eurographics Association. 8

Toolan, T. M. (2006). Open Dynamics Engine v.0.5 users guide. 15

Tu, X. and Terzopoulos, D. (1994). Artificial fishes: Physics, locomotion, perception, behavior. In *Proceedings of the 21st Annual Conference on Computer Graphics and Interactive Techniques (ACM SIGGRAPH)*, pages 43–50. ACM. 6

Wilhelms, J. and Gelder, A. (1997). Anatomically based modeling. In *Proceedings of the 24th Annual Conference on Computer Graphics and Interactive Techniques (ACM SIGGRAPH)*, pages 173–180. ACM Press/Addison-Wesley Publishing Co. 6, 7

Wu, J. and Popović, Z. (2003). Realistic modeling of bird flight animations. In *ACM SIGGRAPH 2003*, pages 888–895. ACM. 6

Yin, K., Loken, K., and Panne, M. (2007). Simbicon: Simple biped locomotion control. *ACM Transactions on Graphics*, 26. 6

Zhao, J. and Badler, N. (1994). Inverse kinematics positioning using nonlinear programming for highly articulated figures. *ACM Transactions on Graphics*, 13:313–336. 4

Zhou, X. and Lu, J. (2005). NURBS-based Galerkin method and application to skeletal muscle modeling. In *Proceedings of the 2005 ACM Symposium on Solid and Physical Modeling*, pages 71–78. ACM. 7

Zordan, V., Celly, B., Chiu, B., and DiLorenzo, P. (2004). Breathe easy: Model and control of simulated respiration for animation. In *Proceedings of the 2004 ACM SIGGRAPH/Eurographics Symposium on Computer Animation*, pages 29–37. Eurographics Association. 7